

# Southern Nicola Arc Project (SNAP): Preliminary results

Mitchell G. Mihalynuk<sup>1, a</sup>, James M. Logan<sup>1</sup>, Larry J. Diakow<sup>1</sup>, Richard M. Friedman<sup>2</sup>, and Janet Gabites<sup>2</sup>

<sup>1</sup> British Columbia Geological Survey, Ministry of Energy and Mines, Victoria, BC, V8W 9N3

<sup>2</sup> Pacific Centre for Isotopic and Geochemical Research, Department of Earth, Ocean and Atmospheric Sciences, University of British Columbia, Vancouver, BC, V6T 1Z4

<sup>a</sup> corresponding author: Mitch.Mihalynuk@gov.bc.ca

Recommended citation: Mihalynuk, M.G., Logan, J.M., Diakow, L.J., Friedman, R.M., and Gabites, J., 2014. Southern Nicola Arc Project (SNAP): Preliminary results. In: Geological Fieldwork 2013, British Columbia Ministry of Energy and Mines, British Columbia Geological Survey Paper 2014-1, pp. 29-57.

---

## Abstract

Geological field studies in 2013 took advantage of new access and exposures from extensive clear-cut timber harvesting between Princeton and Tulameen. Revision mapping and laboratory investigation reveal new facets of the prolifically mineralized Nicola arc. <sup>40</sup>Ar/<sup>39</sup>Ar cooling and U-Pb crystallization ages show that volcanism, long considered restricted to the Late Triassic, extends into the Early Jurassic. Volcanism changes near the Triassic-Jurassic boundary from feldspar-pyroxene ± olivine-phyric, to hornblende as an accessory or even principal phenocryst phase, perhaps indicating a change to more hydrated magma sources. Felsic volcanic rocks interpreted as part of the Nicola arc occur north of Princeton and near Tulameen, where a bimodal submarine succession contains previously unreported, possible exhalite horizons with copper mineralization. A northerly trending high-strain zone can be traced intermittently for ~ 20 km. It bisects the study area, with strain focused in calcareous strata. Extensive uplift and erosion of the Nicola arc, including its plutonic roots, preceded deposition of the Spences Bridge Group (middle Cretaceous). This volcanosedimentary succession, less than 500 m thick, includes ignimbrite and rhyolite flows not found elsewhere. In the early Eocene, down-to-the-west extension faulting is associated with syn-deformational silicic volcanism. One of these faults, the Boundary Fault, marks the western limit of copper-gold porphyry mineralization at both Copper Mountain and Miner Mountain. Deformation caused brecciation of the basin strata and offset alkali olivine basalt dikes interpreted as feeders to Miocene plateau lavas. Accurate reconstruction of geological events since the Late Triassic is a critical aid to finding offset portions of known porphyry deposits as well as successful exploration for undiscovered deposits.

**Keywords:** Geology, porphyry copper gold, volcanogenic massive sulphide, Miner Mountain, Axe, Princeton, Tulameen, Nicola Group, Spences Bridge Group, paleogeography

---

## 1. Introduction

The southern Nicola arc, (Quesnel terrane; Fig. 1) has been a mainstay for copper-gold production in British Columbia for 50 years. Taking advantage of new access and exposures from extensive clear-cut timber harvesting, the Southern Nicola Arc Project (SNAP) builds on pioneering studies by Preto (1979) and Monger (1989) and is designed to illuminate new opportunities in this prolific mining camp. The project focuses on areas where new information is most likely to expand the existing geological foundation and links to the most recent systematic mapping in the southernmost Nicola Group by Massey and Oliver (2010). SNAP aims to fine tune the stratigraphic, structural, and mineral deposit evolution of the Nicola arc between Princeton and Merritt (Figs. 1, 2), through 1:20 000-scale geological mapping and application of modern geochronologic and paleogeographic reconstruction methods.

Following a scoping study in 2012 (Fig. 3; Mihalynuk and Logan, 2013a, 2013b), we initiated systematic mapping in NTS 92H/9W and 10E, extending into 7W as far south as the Similkameen River (see Massey and Oliver, 2010, and Mihalynuk and Logan, 2013a for summaries of previous geologic investigations). This paper presents the preliminary stratigraphic, geochronologic and major structural elements as the first steps toward reconstructing the Late Triassic mineralizing landscape.

## 2. Geography and geological setting

Rocks of the southern Nicola arc are sparsely exposed on the dissected plateau between the Coast-Cascade ranges and orographic desert of the Interior Plateau (Fig. 1). Local extensive exposures are along ridges and steep valley walls. Mainly dry open pine forests, minor grasslands, and many small lakes make for ideal cattle rangeland and easy foot travel.

The southern Nicola arc and underlying basement rocks belong to the Quesnel terrane, a composite island arc that initiated at the western margin of ancestral North America in Devonian time (Monger et al., 1972; Monger, 1977; Mihalynuk et al., 1994; Ferri, 1997), on rocks at least as old as Late Silurian; (Read and Okulitch, 1977). Like modern Japan, a back-arc basin formed as Quesnel arc rifted farther from its continental margin homeland (Davis et al., 1978; Tempelman-Kluit, 1979; Ferri, 1997). As the back arc basin grew to oceanic proportions, Quesnellia became isolated enough from North America to permit the colonization of endemic organisms, the fossil remains of which are lacking in now adjacent parts of cratonic North America, but are found to the west in Stikine terrane (Ross and Ross, 1983 and 1985). Both Quesnel and Stikine terranes were repatriated with North America by Early to Middle Jurassic (Ricketts et al., 1992; Nixon et al., 1993; Mihalynuk et al., 2004;) as they buckled against the margin, capturing exotic oceanic rocks of the Cache Creek terrane between them (Monger and Ross, 1971; Mihalynuk et al.,

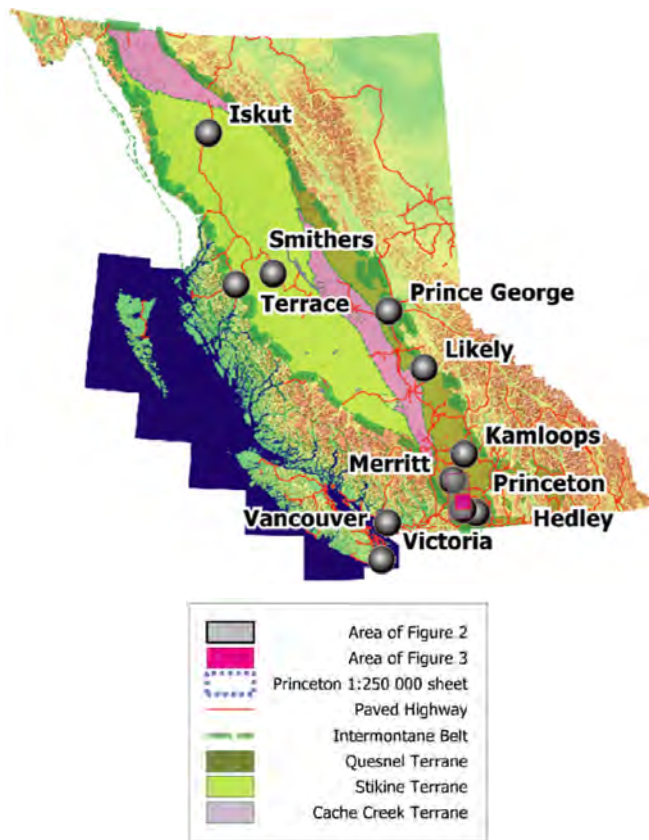


**Fig. 1.** Physiographic and tectonic setting of the Southern Nicola Arc Project (SNAP) study area between Princeton and Merritt.

1994). Since Middle Jurassic time, rocks of the Quesnel arc were deformed during collisions that shuffled rocks along the ancestral continental margin southward and then northward, coming to rest in the Eocene (Enkin, 2006; Sigloch and Mihalynuk, 2013).

Eocene extension in the southern Cordillera (Brown and Journeay, 1987) gave rise to the landscape from which the modern topography was inherited, with relatively minor modification by Quaternary glaciation (Tribe, 2005). Accurate reconstruction of the prolifically mineralized Late Triassic arc cannot be achieved without restoring the effects of Jurassic to Eocene (and younger?) deformation.

### 3. Stratigraphy

Four main volcanosedimentary assemblages, each with comagmatic intrusions, are exposed in the SNAP study area (Figs. 2, 3): the Nicola Group; the Spences Bridge Group (middle Cretaceous); the Princeton Group (Eocene); and Miocene-Pliocene plateau basalts (Monger, 1989; Preto, 1979). New geochronologic data presented herein (see below) demonstrate that parts of the Nicola Group, hitherto considered Late Triassic, extend into the Early Jurassic.

#### 3.1. Nicola Group

The southeastern and northeastern extents of the Nicola Group in the current study area are part of the “Eastern Belt” of Preto (1979). Summarizing after Mihalynuk and Logan (2013a, 2013b): in the north, a lower succession of volcanoclastic

strata derived from coarse augite porphyry breccia is overlain by coarse augite-hornblende porphyry. They are intruded by mineralized synvolcanic intrusions. All magmatic rocks show geochemical characteristics typical of arc parentage (Fig. 4, see also below). Polymictic conglomerate derived from these rocks overlies, and is intercalated with the youngest augite-hornblende-phyric volcanic rocks. In the south, at Miner Mountain, the lower coarse augite porphyry units are not well represented. Instead, tuffaceous carbonate at the lowest structural levels (found mainly in drill core), pass upward into medium- and fine-grained feldspar- and pyroxene- ± olivine-phyric flows and pyroclastic rocks, and finally into coarse hornblende-pyroxene-feldspar porphyry breccia. As in the north, thick polymictic epiclastic strata apparently cap the succession. They consist of angular pyroxene- or pyroxene-hornblende fragments in massive layers tens of metres thick. This suggests that volcanism was synchronous with sedimentation. Because clasts in the conglomerate can reach almost a metre in diameter and match those in the underlying arc, they are interpreted as arc-proximal. Mafic rocks invariably display an authigenic epidote-chlorite-actinolite ± prehnite assemblage typical of low-grade regional depth-controlled hydrothermal metamorphism in Cordilleran volcanic terranes (Cho and Liou, 1987; Mihalynuk and Ghent, 1996). However, intercalations of sedimentary strata are common, and it is likely that crosscutting intrusions maintained a geothermal gradient to generate greenschist mineral assemblages, and that distal or shallow strata of very low grade have been eroded or structurally removed.

Below we describe units of regional importance not described in (Mihalynuk and Logan, 2013a, 2013b).

#### 3.1.1. Tabular feldspar porphyry clast-bearing heterolithic breccia

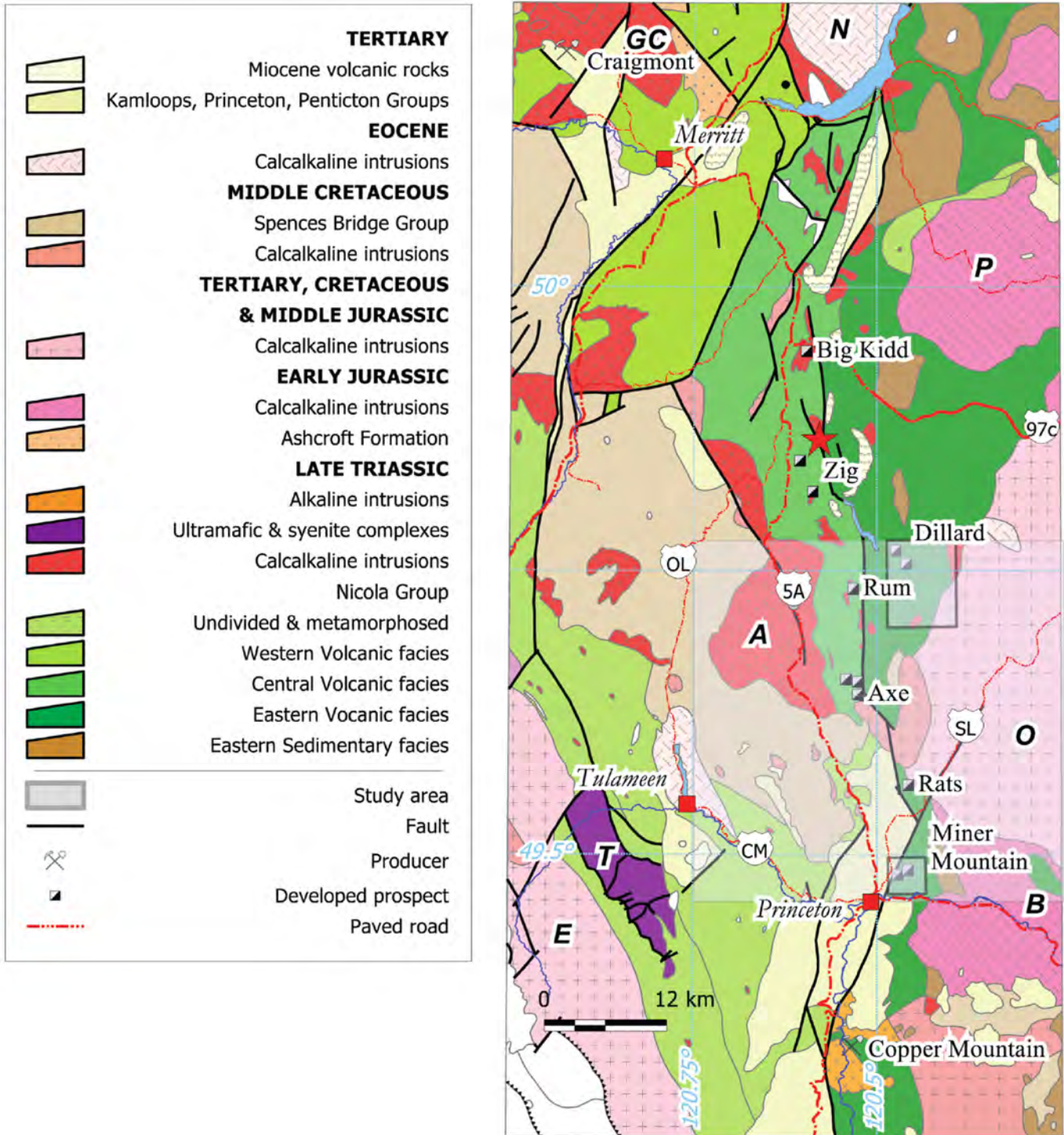
One of the most widespread units in this part of the Nicola arc consists of heterolithic breccia that contains clasts of tabular feldspar porphyry, and intercalations of lahar and tuffite derived from coeval arc strata. In the relatively well-exposed highland north of Missezula Mountain (Fig. 3), this unit is probably at least 300 m thick. Because of abrupt volcanic and sedimentary facies changes we have grouped several different lithologies into the one unit.

Outcrops weather light to dark green-grey; greenschist alteration produces fresh surfaces that are usually bright green. Coarse breccia is the most common lithology; in lesser lapilli tuff, tabular feldspar is typically the most abundant phenocryst, but either pyroxene or hornblende and pyroxene (hornblende:pyroxene about 1:1 to 5:1) is also present.

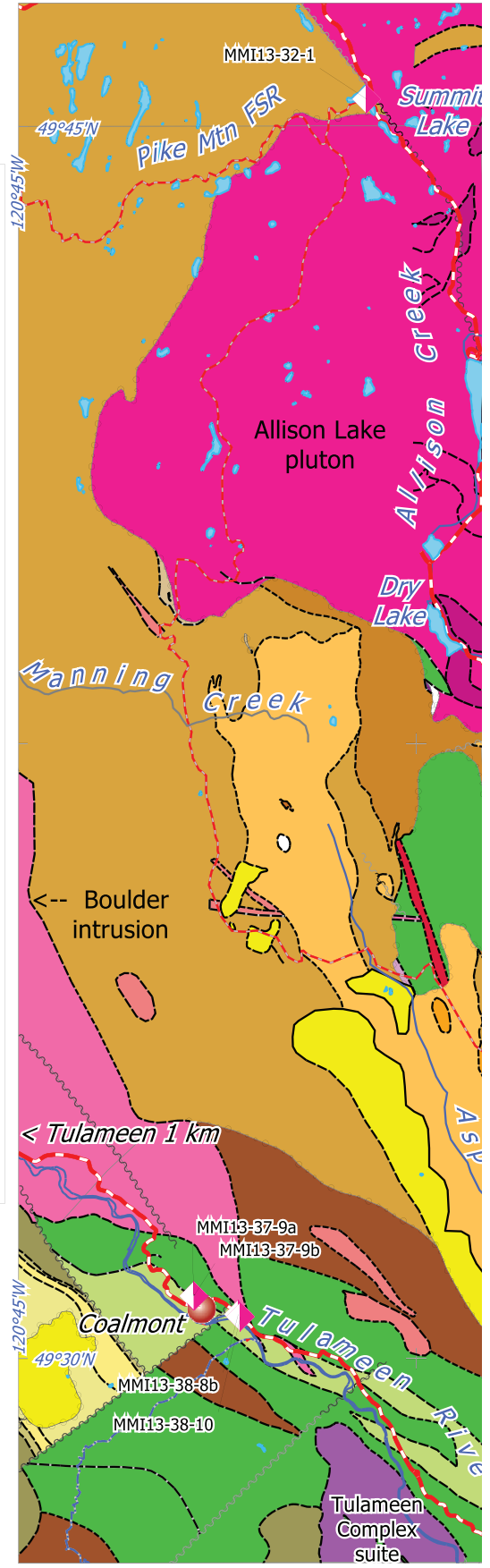
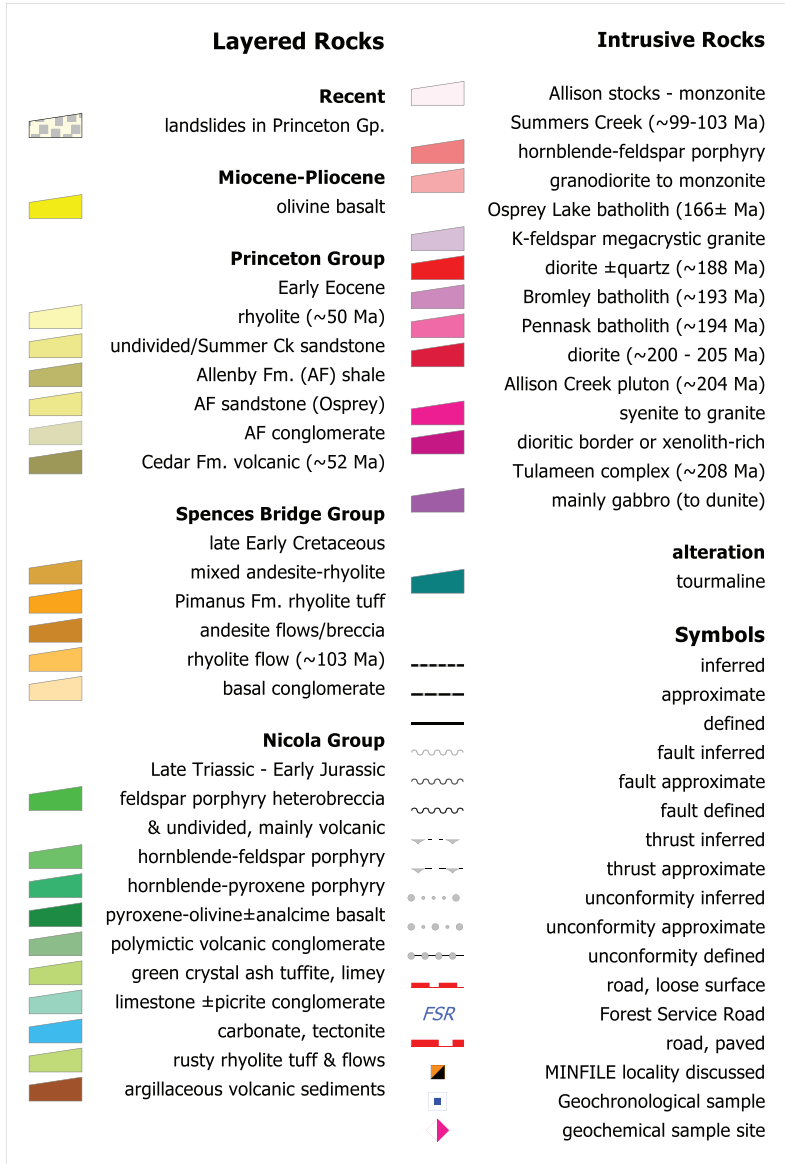
Reworked equivalents of fragmental deposits produce boulder to granule conglomerate with indistinct to well-developed bedding. Grading and dewatering structures are common. Clasts derived from outside the local volcanic environment include limestone, diorite, and hornblende-feldspar porphyry. Carbonate is a common matrix constituent. Local, decimetre-thick, discontinuous beds of poorly fossiliferous limestone suggest deposition of part of the succession in a marine environment.

#### 3.1.2. Rusty rhyolite lapilli tuff

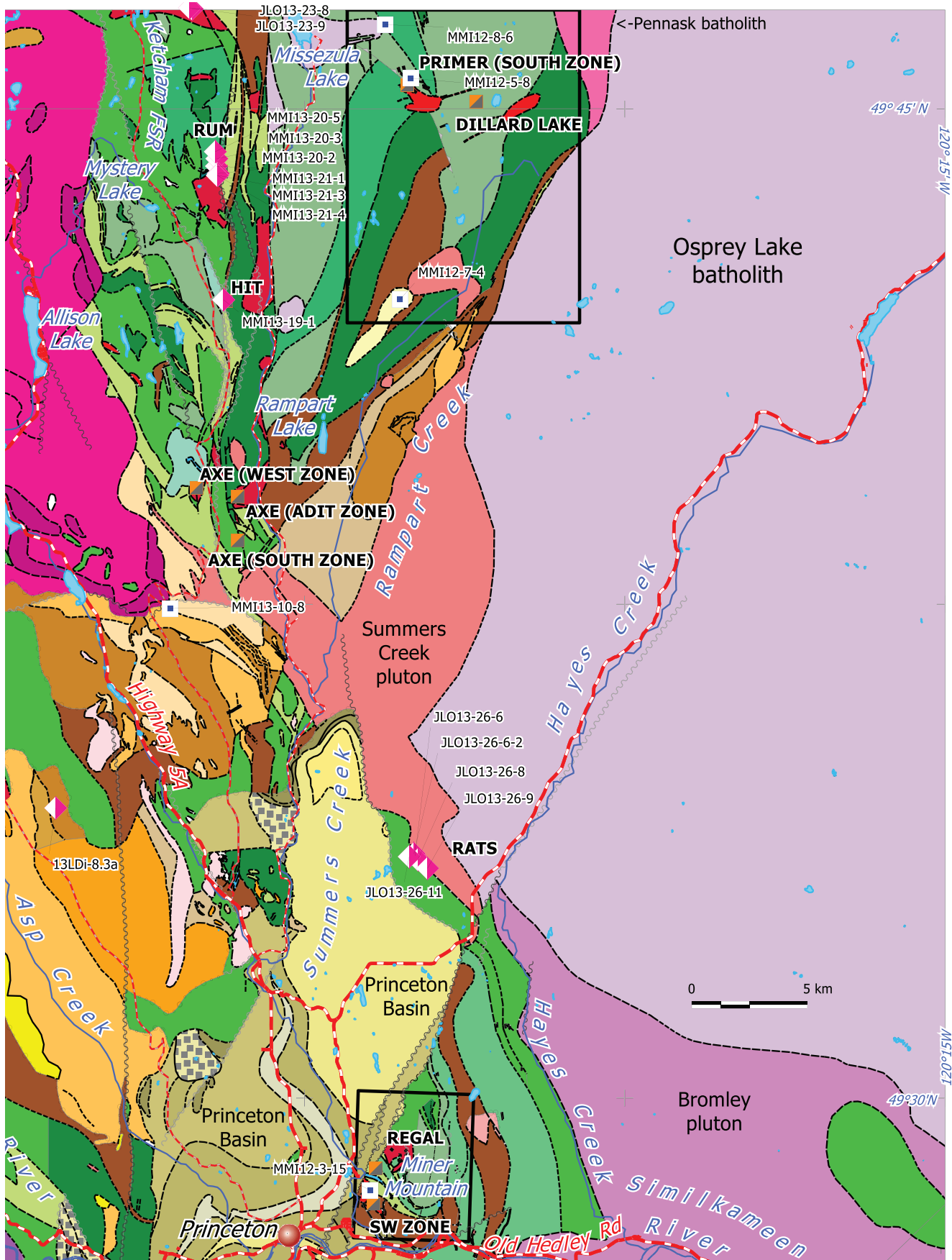
Pyritiferous lapilli tuff forms a kilometre-wide belt north of



**Fig. 2.** Geological setting of 2013 field mapping, Southern Nicola Arc Project (SNAP), between Princeton and Merritt. Extents of Preto's Western belt (mafic submarine volcanic and sedimentary rocks), Central belt (arc axis, mafic volcanic and coeval intrusive rocks) and Eastern belt (intermediate to felsic volcanic and sedimentary rocks) are shown for reference, as adapted from Massey et al. (2005). Abbreviations denote major plutons: A = Allison Lake, B = Bromley, BI = Boulder intrusion, E = Eagle, GC = Guichon Creek, N = Nicola, O = Osprey Lake, P = Pennask, S = Summers Creek, T = Tulameen Complex. See Figure 1 for context.



**Fig. 3.** Simplified geology of the Summers Creek area (NTS mapsheets 92H/9W and 10E and adjacent parts of sheets to the north and south). Compilation includes geological information from Monger (1989, regional framework), Preto (1979, mainly including areas adjacent and between Highway 5A and Summers-Rampart creeks), Massy and Oliver (2010, southwest of Tulameen River), McMechan (1983, margins of the Princeton basin), Massey (2000, Princeton basin interior), and SeGo! Resources Inc. (unpublished data from within 5 kilometres of Miner Mountain). More detailed geology of the boxed areas can be found in Mihalynuk and Logan (2013a) for the southern boxed area around Miner Mountain, and Mihalynuk and Logan (2013b) for the northern boxed area around Dillard Lake and Primer prospects. See Figure 2 for context.



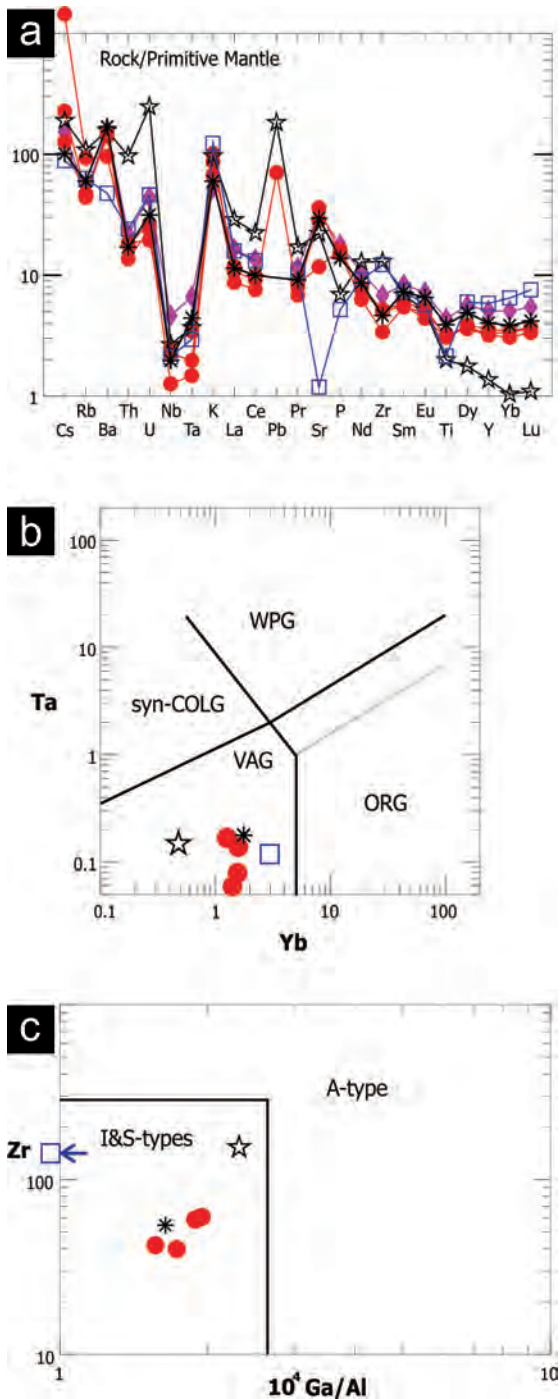


**Fig. 4.** Geochemical characteristics of felsic members of the Nicola arc and younger strata. **a)** Primitive mantle normalized extended trace element plot (Sun and McDonough, 1989), solid red circles are dioritic intrusions of mainly Early Jurassic age, asterisk is mineralized granodiorite at the Axe deposit, solid purple diamond is mafic volcanic breccia with diorite fragments, open blue square is the foliated Axe ignimbrite, open black star is Eocene Princeton Group rhyolite. **b)** Ta-Yb plot with fields after Pearce et al. (1984). **c)** Zr vs  $10^4 \text{ Ga/Al}$  fields discriminate anorogenic granitoids (A-type) from orogenic granitoids generated from igneous or sedimentary source rocks (I and S types) after Whalen et al. (1987).

the Axe deposit (Fig. 3), where orange and cream-weathering quartz-sericite schist contains flattened lapilli-sized white-mica-rich patches, interpreted to be collapsed pumice fragments. This lithology passes northward abruptly into weakly to unfoliated, rusty-weathering, pyritic, felsic lapilli tuff. Phenocrysts are limited to ghost feldspars (originally sanidine?), that are now altered to clay minerals. A possible equivalent is exposed south of the Axe deposit, where quartz-eye tuffs are adjacent to a several-metre-thick fossiliferous carbonate unit.

Between Princeton and Tulameen, rhyolitic ( $\pm$  mafic) rocks that may correlate with those near the Axe deposit, form a belt  $> 10$  km long and  $< 2$  km wide. East of Coalmont (Fig. 3), a belt of pyritic, sparsely quartz-phyric, white mica and clay-altered rhyolite lacks definitive extrusive textures. This unit could be a hypabyssal sill related to the Boulder intrusion, which displays border phases that are lithologically identical (see below). A similar unit, speculated to be at approximately the same stratigraphic level, outcrops farther northwest, between Coalmont and Tulameen. Where best exposed in roadcuts, it includes rhyolite blocks nearly a metre across, floating in an altered, dark grey ash matrix, that locally grades into felsic lapilli tuff. Some cherty fragments containing polycrystalline quartz grains the size of radiolaria are interpreted as biogenic. Beds of granulestone with mainly embayed quartz clasts (Fig. 5a) are in a part of the section containing finely laminated cherty layers with pyrite and chalcopyrite that are interpreted as exhalite (Fig. 5b). This succession is bimodal; basaltic pillow breccias (Fig. 5c) point to a submarine depositional setting.

Like other intrusive and volcanic samples of the Nicola Group, a sample of rhyolite (MMI12-11-15, north of the Axe deposit, Fig. 3) displays geochemical characteristics of arc parentage (Fig. 4a). It is metaluminous, with elevated Large Ion Lithophile elements (LIL) and depleted in Ta, Nb and Ti, and shows minor enrichment of Heavy Rare Earth Elements (HREE) (Mihalynuk and Logan, 2013c). Strong depletion of the relatively mobile element Sr (25 ppm), and to a lesser extent, Ba and P (333 ppm and 0.11%  $\text{P}_2\text{O}_5$ ), is attributed to alteration. Typical unaltered rhyolite displays Sr that is an order of magnitude more abundant at similar Rb concentrations (40 ppm) (Halliday et al., 1991). Using trace element discrimination criteria, the rhyolite shows characteristics of arc-related (Fig. 4b) orogenic (Fig. 4c) granitoids. The rusty ignimbritic tuff is distinguished from Princeton Group rhyolites, which have strong HREE depletions.

The rusty tuff and rhyolite lapilli tuff units are significant in that they show that felsic volcanic rocks extend from the Western facies belt, where rhyolitic rocks are a hallmark, to the eastern facies belt, where they are not well known. However, attempts to extract zircons for U-Pb geochronology from the foliated "ignimbrite" that would verify correlation, have been unsuccessful.

Regardless of age, the submarine volcanic rocks are important because they represent an environment where volcanogenic massive sulphides can accumulate. Positive indicators are: quartz-sericite alteration such as displayed by foliated lapilli flattened into a strong phyllitic fabric west of the Tulameen River at Coalmont (Fig. 6c) and traces of copper mineralization east of the river (as noted above) in which felsic volcanic strata containing reworked quartz eyes (Fig. 5a) are intercalated with laminated cherty layers containing pyrite, chalcopyrite (stained

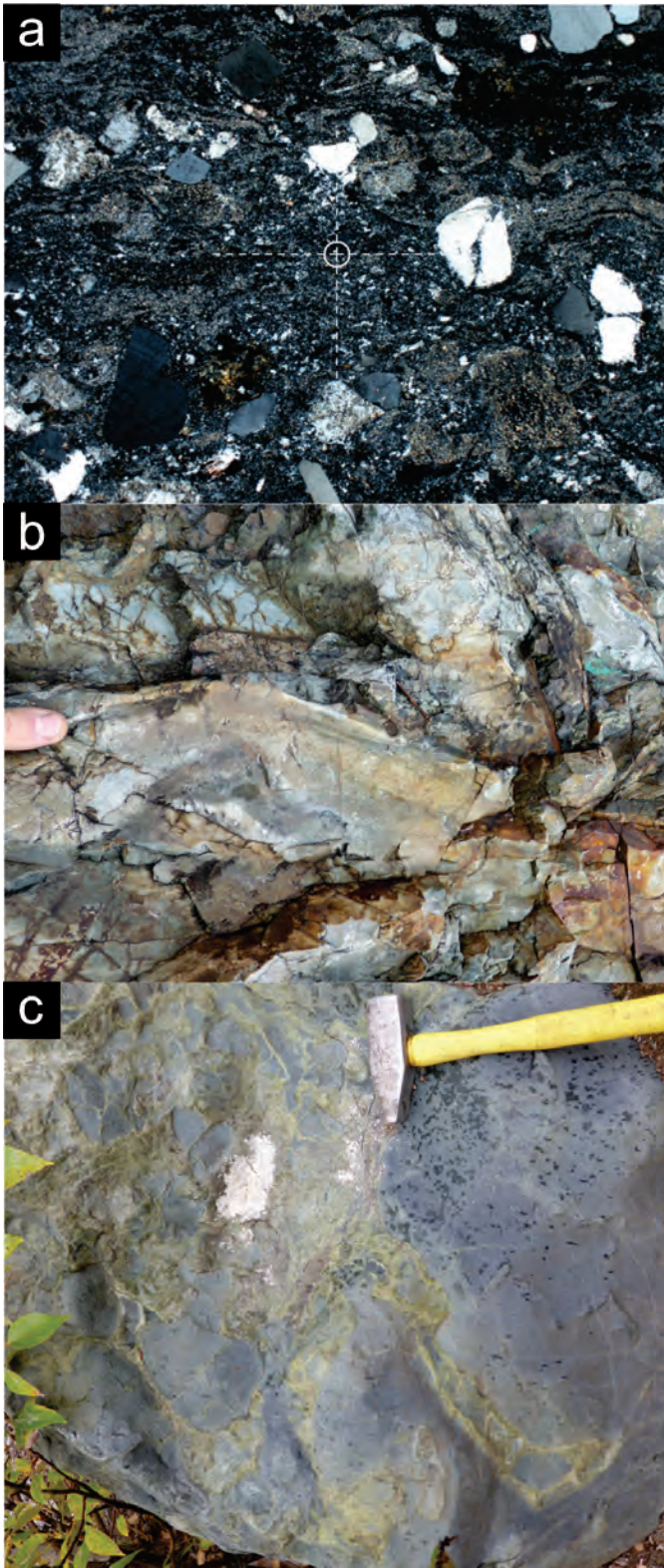


**Fig. 5.** Examples of Nicola Group units from a submarine bimodal succession near Coalmont. Top = epiclastic. Middle = cherty tuff. Bottom = pillows. **a)** Photomicrograph of an epiclastic layer showing rounded and embayed quartz grains (circle at cross hairs has a radius of 100  $\mu\text{m}$ ). **b)** Laminated light green and rust-weathering cherty tuff is mineralized with pyrite and minor chalcopyrite. **c)** Strongly epidote-altered pillow breccia.

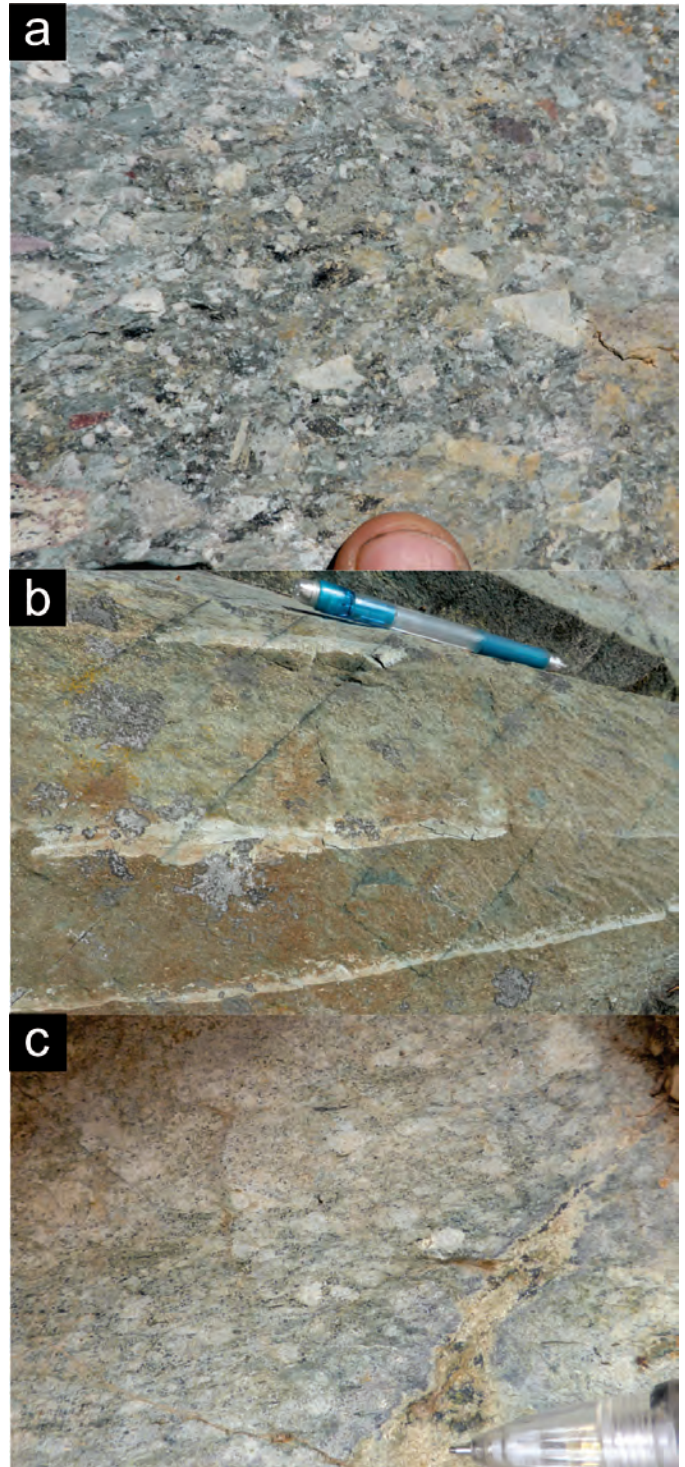


**Fig. 6.** Tuffite correlated with the Nicola Group. **a)** Lapilli tuff with angular sparsely quartz-phyric felsic fragments. **b)** Well-bedded and calcareous crystal ash tuffite. **c)** Felsic tuff near Coalmont is similar to **a)** but is altered by white mica and is foliated.

by malachite-azurite bloom in Fig. 5b) that may have formed near an exhalative vent.

### 3.1.3. Carbonate tectonite

Tectonized carbonate rocks outcrop in a linear belt along the

western rim of the Summers Creek valley. The belt is generally less than 20 m wide, as exposed or estimated from regional dips and map patterns. In most places, limestone is well foliated and folded, but it can be massive and recrystallized, especially near the middle of the unit. South of the Axe, it crops out between volcanogenic quartz-bearing sandstone and mafic tuffaceous rocks. North of the Axe, near Mystery Lake, it is flanked to the east by a foliated limestone-boulder conglomerate with a matrix of feldspar, pyroxene, and olivine-phyric tuff. Along strike, the unit grades into well cleaved, maroon, calcareous volcanic sandstone. The western contact of the tectonite unit is covered, but must lie within 10 m of phyllitic tuffaceous siltstone, which contains auriferous quartz veins at the Hit prospect (see below). At one locality near Mystery Lake (Fig. 3) its upper (eastern) contact is an erosional unconformity beveled beneath conglomerates containing boulders and cobbles of limestone (see below).

### 3.1.4. Limestone and picrite clast-bearing conglomerate

Immediately east of the Ketchan Road, near Mystery Lake, an approximately 30 m-thick conglomerate unit containing cobbles and boulders of limestone rests unconformably on the tectonized limestone unit. Cobbles and small boulders of coarse augite and augite-olivine porphyry (loosely referred to as picrite) are of secondary abundance. Some olivine-bearing clasts also contain sparse rounded pink phenocrysts < 5mm in diameter that may be altered analcime or leucite. A scattering of well-rounded cherty red tuff cobbles are notable, as they are unaffected by the foliation into which the carbonate, and to a lesser degree, the picritic clasts are flattened. Foliation is most strongly developed in the matrix, which is composed of mixtures of carbonate and picritic detritus, possibly tuff.

Overlying the basal conglomerates are very well bedded polymictic conglomerate and sandstone beds displaying water escape structures and clastic dikes. Pyroxene ± analcime-porphyrific hyaloclastite layers several metres thick point to synvolcanic deposition. Traces of copper mineralization are ubiquitous, with one sample returning 0.34% Cu, 1.7 ppm Ag and 20 ppb Pd (MMI13-17-11, Table 1).

This conglomerate unit is only locally developed, suggesting deposition on an irregular paleosurface. Across Summers Creek valley to the southeast, pyroxene and olivine-rich sandstone beds centimetres-thick occur in a conglomerate-rich sedimentary succession at least 500m thick. Coarse, magnetite-rich gabbro clasts suggest that both the deepest (gabbroic roots) and shallowest (olivine-bearing extrusive units) arc levels were exposed to erosion at this time.

### 3.1.5. Acicular hornblende porphyry

About 40 m of coarse trachytic hornblende porphyry lies above the conglomeratic unit, but its lower contact is covered. Hornblende comprises ~ 20% of the unit and can reach 1.5 cm long, although it is typically < 0.5 cm and aligned in a pervasively chlorite-epidote altered, green-grey matrix. Generally the hornblende phenocrysts are less altered, and are locally vitreous.

Cobbles of hornblende porphyry in an overlying conglomerate suggest that sedimentary reworking was coeval with volcanism. The conglomerate passes eastward and probably upsection, into medium-grained feldspar and pyroxene > hornblende-

phyric breccia.

### 3.1.6. Felsic tuffite

Well-bedded and moderately to unfoliated ash and lesser lapilli tuff underlies low, glacially sculpted ridges in a clear cut between Missezula and Mystery lakes. Contact relationships with layered strata of the Nicola Group could not be established; however, the lowest level of the section is apparently a nonconformity with altered diorite. Tight, near vertical folds repeat the section, which appears to have been originally ~ 200 m thick. The most characteristic units are coarse felsic ash tuffite, and green ash and crystal tuffite. Other minor beds include polymictic conglomerate with mainly limestone pebbles in a matrix of tuffaceous wacke with conspicuous coarse quartz grains.

Massive beds of felsite tuffite consist of angular, white to dark green, coarse ash to lapilli-sized clasts (Fig. 6a) and grade into thinner beds with sand-sized grains of similar composition. Most fragments are aphanitic or very fine-grained, but some contain up to 30% feldspar, interpreted from simple twinning to be sanidine, and sparse medium-grained quartz.

Of similar thickness is an adjacent unit of green ash and crystal tuffite that is very well bedded (Fig. 6b), with beds typically centimetres to decimetres thick. Flame structures, graded bedding, scours, and soft-sediment gravity slides are common. Lithic fragment and feldspar crystal-bearing sandstone and siltstone have a calcareous cement.

Although the felsite tuffite unit is similar to the Skwel Pecken Formation (Early to Middle Jurassic) defined near Hedley (Ray and Dawson, 1994), we provisionally include it in the Nicola Group, following Preto (1979). The unit resembles distal facies of the rusty tuff and rhyolite lapilli tuff unit described above (compare Figs. 6a and b).

## 3.2. Spences Bridge Group

Spences Bridge Group units define a continuous, narrow belt that extends 180 kilometres northwest from Princeton (Fig. 2). During regional mapping near Princeton, Rice (1960) recognized two Lower Cretaceous volcanic sequences, the Spences Bridge Group and the overlying Kingsvale Group. The term 'Kingsvale' was later abandoned (Monger, 1989) and the Spences Bridge Group was formally divided into the Pimainus Formation and the overlying Spius Formation from detailed work near Gillis Lake south of Merritt (Thorkelson and Rouse, 1989). In 2001 and 2002, soil sampling and prospecting by Strongbow Exploration near Lytton and Merritt led to discovery of the first known epithermal vein-style mineralization in the Spences Bridge Group. Diakow and Barrios (2008, 2009) refined the geology at the type area near Gillis Lake, and expanded it to adjacent areas near notable epithermal gold occurrences.

In the study area, the Spences Bridge Group unconformably overlies the Nicola Group and related plutons adjacent to Allison Creek and Highway 5A. The unconformity, generally concealed by vegetation, is represented by a basal conglomerate containing Triassic granite clasts. We recognize three volcanic facies above the basal conglomerate, based on a near-continuous section that extends from Dry Lake, along Highway 5A, then westward onto the plateau (Fig. 3). The lowest facies consists of compositionally uniform feldspar ± pyroxene andesite

**Table 1.** Selected elements from the suite analyzed by Inductively Coupled Plasma – Mass Spectroscopy (ICP-MS). A complete array of elements analyzed, plus determinations by Instrumental Neutron Activation Analysis are reported in Mihalynuk et al. (2014). UTMIs are Zone 10, NAD 83.

Lab No.	Station No.	UTME	UTMN	Ag	As	Au	Cd	Co	Cu	Fe	Hg	Mn	Mo	Ni	Pb	Pt	S	Zn	
				ppb	ppm	ppb	ppm	ppm	ppm	%	ppb	ppm	ppm	ppm	ppm	ppb	ppb %	ppm	
62353	JLO13-1-9	684666	5486546	333	10.4	4.2	0.13	19.6	128.65	5.56	2138	697	0.63	7.4	12.23	15	6	3.00	51.7
62354	JLO13-6-6	685374	5512460	6	1.5	<0.2	0.15	8.8	2.85	1.42	7	669	0.07	3.8	2.50	<10	<2	<0.02	46.4
62355	JLO13-6-10	685323	5513423	164	1.4	3.2	0.05	17.3	255.07	3.74	8	486	0.30	6.8	0.31	<10	3	0.02	45.4
62356	JLO13-6-11	685552	5513493	276	1.8	3.9	0.08	21.5	381.44	1.54	30	454	0.22	8.6	0.95	16	4	0.25	21.9
62357	JLO13-8-2	681596	5513260	45	3.4	0.9	0.33	22.5	187.51	4.26	29	1249	0.10	16.9	4.56	<10	<2	<0.02	70.5
62358	JLO13-10-7	679167	5495695	113	1.4	<0.2	0.02	16.6	61.50	3.20	<5	517	0.27	8.1	3.43	<10	2	1.20	42.7
62359	JLO13-11-10	676088	5500643	177	3.6	6.8	0.03	3.2	2.88	3.99	36	990	4.09	1.0	1.15	<10	<2	1.23	103.9
62360	JLO13-11-11	676113	5500372	77	5.0	0.7	0.04	10.8	52.24	4.08	22	141	7.57	1.9	1.75	<10	<2	2.36	16.9
62361	JLO13-12-9	675096	5506753	51	5.3	1.8	0.01	56.5	26.28	10.94	<5	2993	0.65	18.3	0.68	<10	5	4.16	138.5
62362	JLO13-12-21	674985	5502908	3540	1.0	7.1	1.61	46.0	5870.03	2.95	1017	825	1.69	31.2	1.23	<10	3	0.19	35.7
62363	JLO13-10-16-2	678534	5491973	15310	29.0	7.1	16.36	33.5	>10000.00	16.88	55	978	11.23	109.1	33.32	<10	5	0.06	2291.6
<b>Log prospect</b>																			
62364	JLO13-23-8	676833	5516535	19074	<0.1	975.2	1.14	27.1	>10000.00	6.61	312	1183	0.33	9.3	60.95	58	35	0.20	141.3
62365	JLO13-23-9	676763	5516564	148	5.0	59.9	0.12	16.0	2140.69	4.22	38	747	0.97	1.3	4.72	323	22	0.13	71.5
<b>RATS prospect</b>																			
62366	JLO13-26-6	683900	5492971	729	16.1	6.9	5.96	26.4	983.46	4.30	21	1767	1.25	64.8	19.40	<10	<2	<0.02	582.5
62367	JLO13-26-6-2	683868	5493033	17278	2.7	41.1	663.19	38.8	>10000.00	18.13	<5	1539	28.86	59.5	36.15	<10	3	0.04	>10000.0
62368	JLO13-26-8	683984	5492864	11134	6.9	6.4	1.44	44.5	7591.77	4.92	148	1798	123.21	70.7	25.81	11	<2	0.31	135.6
62369	JLO13-26-9	684266	5492632	5599	8.5	30.7	0.56	33.1	6370.60	4.82	71	1061	19.70	4.6	38.59	17	5	<0.02	274.4
62370	JLO13-26-11	683738	5492942	2244	9.4	3.0	0.58	40.3	4869.99	4.38	29	969	90.55	7.9	11.32	<10	3	0.12	79.5
62371	STD till#1750 -	-	-	265	16.5	19.0	0.21	14.4	45.53	3.31	108	1183	0.70	19.7	16.50	<10	<2	<0.02	68.4
62372	13LDi-7.5	672627	5497504	24	1.3	0.3	0.08	1.5	3.39	1.21	<5	647	0.53	0.7	13.40	<10	<2	<0.02	51.1
<b>Epithermal vein</b>																			
62373	13LDi-8.3a	673718	5493984	122	0.2	<0.2	1.17	4.8	55.48	0.99	<5	694	3.87	31.2	24.99	<10	<2	<0.02	164.2
62374	13LDi-8.3b	673718	5493984	170	0.7	<0.2	1.19	5.3	151.18	0.91	<5	585	10.30	37.1	19.57	<10	<2	<0.02	126.8
62375	13LDi-8.3c	673718	5493984	205	0.2	<0.2	0.99	1.8	55.94	0.37	<5	384	1.78	5.7	61.00	<10	<2	<0.02	69.6
62376	MHE13-18-6	677040	5511769	179	0.8	2.0	0.02	7.0	137.86	2.09	<5	276	0.39	10.5	3.15	<10	<2	0.10	17.3
62377	MHE13-19-10	679209	5507702	79	4.6	1.5	0.05	33.4	101.77	4.76	12	747	0.97	12.6	1.23	<10	7	0.61	40.3
62378	MHE13-24-2	669125	5488241	54	0.7	0.3	0.03	30.0	105.86	4.29	<5	804	0.41	7.0	0.31	<10	<2	0.11	56.6
62379	MHE13-6-2	685516	5567552	62	4.7	<0.2	0.11	5.2	2.24	2.34	7	679	0.17	2.3	4.43	<10	<2	<0.02	59.0
62380	MM13-2-1	686381	5492520	189	2.0	4.7	0.20	8.2	57.81	2.39	<5	369	0.90	4.7	9.12	<10	<2	0.92	28.5

Table 1. Cont'd.

Lab No.	Station No.	UTME	UTMN	Ag	As	Au	Cd	Co	Cu	Fe	Hg	Mn	Mo	Ni	Pb	Pd	Pt	S	Zn
				ppb	ppm	ppb	ppm	ppm	ppm	%	ppb	ppm	ppm	ppm	ppm	ppb	ppb	%	ppm
62381	MM113-2-2a	686465	5492864	291	<0.1	5.2	0.03	1.0	13.80	0.61	10	12	19.49	1.6	22.47	<10	<2	0.36	4.4
62382	MM113-2-2b	686465	5492864	238	1.3	21.6	0.18	1.6	30.59	0.91	7	278	8.25	2.0	8.71	<10	<2	0.18	34.7
62383	MM113-2-3	685875	5491013	189	0.3	2.5	0.09	27.1	263.92	4.33	<5	796	0.38	16.6	1.76	<10	5	0.11	55.0
62384	MM113-2-6	685726	5490996	1801	5.1	257.0	0.47	21.8	5074.04	2.81	9	940	26.52	7.0	5.35	<10	<2	2.17	112.4
62385	MM113-2-7	685562	5490715	1001	1.8	83.3	0.22	17.4	3287.11	2.98	18	538	4.50	10.0	3.83	<10	5	2.56	47.8
62386	MM113-2-12	686042	5491343	458	6.3	58.2	0.03	3.8	126.68	3.78	96	494	7.00	5.7	3.44	13	4	0.62	42.8
62387	MM113-4-5	683564	5505376	229	1.8	10.6	0.12	5.0	209.96	2.09	<5	505	6.03	2.1	9.92	<10	2	0.20	48.6
62388	MM113-4-7	683659	5505377	92	0.4	3.4	0.01	1.1	6.83	0.95	9	8	7.54	1.1	3.52	<10	<2	0.41	2.0
62389	MM113-7-6b	686742	5511482	6	2.0	<0.2	0.10	2.7	2.10	1.80	<5	1413	4.16	2.5	1.29	<10	<2	<0.02	17.9
62390	MM113-8-4	678061	5498946	35	32.5	0.5	0.08	5.5	4.81	2.56	25	477	1.41	1.3	8.33	<10	<2	<0.02	76.0
62391	MM113-9-11	677006	5498406	40	3.0	0.3	0.08	16.6	32.76	4.37	31	1244	0.26	10.4	5.16	<10	<2	1.25	77.2
62392	MM113-9-12	676945	5498377	59	8.1	1.1	0.10	15.5	30.27	4.72	44	1082	1.33	7.6	5.34	<10	<2	3.27	91.2
62393	MM113-9-13	676755	5498740	122	5.4	1.1	0.17	21.6	73.26	5.51	40	1216	0.94	9.9	6.67	<10	<2	2.62	92.8
62394	STD till#1657	-	-	246	15.8	21.6	0.24	12.7	45.94	2.98	89	1097	0.61	16.5	13.96	<10	<2	<0.02	60.5
62395	MM113-12-2	677618	5500676	52	4.3	5.2	0.04	10.7	53.69	2.18	6	375	0.11	17.9	1.94	<10	<2	<0.02	30.1
62396	MM113-12-4	677434	5501164	62	3.0	1.2	0.04	32.9	104.93	6.34	<5	711	0.14	32.8	0.48	19	5	<0.02	76.2
62397	MM113-17-2	671970	5512050	3	1.0	1.9	3.28	27.1	1.82	3.96	11	1454	0.36	44.2	21.54	<10	9	<0.02	203.8
62398	MM113-17-11	676559	5510905	1718	2.2	5.7	0.53	20.6	3413.78	4.23	67	1221	0.04	5.9	3.05	20	4	0.04	122.4
<b>Hit</b>																			
<b>prospect</b>																			
62399	MM113-19-1	677986	5508413	21659	<0.1	1790.2	144.28	0.8	4.24	0.67	2023	209	4.05	3.4	5176.07	<10	<2	0.62	2848.1
62400	MM113-19-10	677274	5512008	307	13.8	3.1	0.84	11.7	86.71	3.49	363	419	0.36	5.9	37.34	<10	9	1.15	187.2
<b>Rum</b>																			
<b>prospect</b>																			
62401	MM113-19-11	677360	5511985	175	5.2	3.3	0.06	29.0	553.84	6.06	27	318	2.78	16.6	2.66	<10	6	0.74	30.7
62402	MM113-19-12	677456	5511961	45	47.8	7.0	0.08	32.3	199.80	5.42	39	326	1.33	10.8	2.95	<10	7	2.07	13.9
62403	MM113-20-1	677641	5512150	66	28.5	4.2	0.07	10.7	8.38	3.14	38	86	1.69	4.7	9.61	<10	3	0.79	27.0
62404	MM113-20-2	677660	5512154	403	3.4	21.0	0.07	19.1	2681.02	1.76	25	300	3.77	5.8	1.24	<10	6	0.87	15.1
62405	MM113-20-3	677664	5512364	95	1.7	9.7	0.35	6.5	572.59	4.74	11	867	3.64	6.0	1.96	<10	<2	0.06	23.5
62406	MM113-20-5	677616	5512559	1150	11.3	2.1	0.22	26.2	132.78	4.11	53	433	0.66	11.3	24.96	<10	4	3.15	31.8
62407	MM113-21-1	677718	5511951	12580	<0.1	83.8	0.20	7.7	8574.74	4.34	120	835	28.63	5.5	6.60	<10	<2	0.04	149.7
62408	MM113-21-3	677705	5511898	340	5.9	52.4	0.52	23.3	1096.58	3.81	15	966	0.75	52.2	4.47	<10	4	0.50	108.9
62409	MM113-21-4	677693	5511894	792	1.4	388.9	0.15	17.8	1674.74	3.31	17	750	0.81	6.7	2.58	<10	<2	0.14	94.8
62410	MM113-21-7	678003	5511483	572	19.9	8.3	0.35	109.6	266.93	10.79	12	1531	0.48	106.6	5.98	<10	<2	5.23	77.8

Table 1. Cont'd.

Lab No.	Station No.	UTME	UTMN	Ag	As	Au	Cd	Co	Cu	Fe	Hg	Mn	Mo	Ni	Pb	Pd	Pt	S	Zn
				ppb	ppm	ppb	ppm	ppm	ppm	%	ppb	ppm	ppm	ppm	ppm	ppb	ppb	%	ppm
62411	MM113-25-4	686620	5488916	603	0.8	7.5	0.09	32.3	872.69	4.85	6	1326	0.13	5.9	2.14	13	3	<0.02	104.4
62412	MM113-25-6	687116	5489375	202	2.6	2.4	0.09	17.4	343.93	3.65	14	1189	0.64	13.1	2.37	39	4	0.04	70.1
62413	MM113-25-7	687045	5488938	2266	<0.1	2.0	0.26	25.0	8441.80	6.02	<5	1150	0.35	7.6	1.72	<10	<2	0.19	95.7
62414	MM113-26-8	670147	5488585	95	4.3	1.7	0.03	18.3	81.65	4.91	<5	632	0.25	6.8	1.79	<10	4	<0.02	54.8
62415	STD till#1657	-	-	211	16.0	5.7	0.22	12.0	45.46	3.03	69	1079	0.59	15.7	14.75	<10	<2	0.02	55.7
62416	MM113-27-6	669169	5487812	78	1.3	<0.2	0.02	5.9	48.07	2.88	<5	1070	0.13	3.8	1.67	<10	3	0.41	56.7
62417	MM113-27-7	669298	5487861	99	2.0	1.0	0.04	19.7	42.29	3.14	<5	306	0.83	49.5	0.58	<10	4	<0.02	32.7
62418	MM113-27-7b	669298	5487861	264	26.9	0.8	0.71	16.9	31.82	3.67	22	964	1.56	6.0	4.92	<10	<2	0.41	118.3
62419	MM113-27-8	668787	5485336	111	8.4	<0.2	0.10	22.7	193.54	4.38	6	801	0.46	18.1	3.49	17	3	0.65	36.0
62420	MM113-27-10	669339	5485477	32	2.4	0.5	0.04	5.9	7.13	2.49	11	450	0.69	3.4	2.92	<10	<2	0.09	20.9
62421	MM113-27-11	669795	5483651	32	5.0	<0.2	0.02	26.4	59.34	3.30	18	686	0.27	16.9	0.75	<10	3	0.16	39.0
62422	MM113-28-2	683667	5488693	413	1.5	<0.2	0.24	22.2	432.50	2.15	8	952	0.14	13.4	2.29	17	5	0.02	81.7
62423	MM113-29-4	672572	5483280	146	2.3	<0.2	0.30	0.9	24.55	2.39	73	264	1.22	1.2	10.75	<10	<2	0.29	96.1
62424	MM113-31-5	669264	5503003	116	1.4	14.6	0.08	6.9	54.84	3.18	9	140	1.65	2.6	1.63	<10	<2	1.06	23.4
<b>Epithermal vein</b>																			
62425	MM113-32-1	669943	5514124	6309	246.4	116.6	0.06	24.3	52.72	5.20	80	4368	3.14	47.9	12.51	<10	<2	3.02	30.8
62426	MM113-37-8	666620	5487206	893	0.5	8.2	0.09	11.0	6636.65	1.06	75	71	5.90	5.8	0.70	<10	<2	0.29	5.1
<b>Possible exhalative mineralization</b>																			
62427	MM113-37-9a	666872	5487010	564	0.3	4.0	0.27	10.7	2932.69	1.31	<5	382	3.82	58.7	0.16	13	<2	0.04	23.9
62428	MM113-37-9b	666872	5487010	124	0.6	6.4	0.02	49.3	81.42	5.39	12	362	2.37	106.5	0.81	<10	7	2.51	38.6
62429	MM113-38-8b	667894	5486628	871	<0.1	4.3	0.07	5.3	3376.03	0.82	39	49	5.37	5.6	0.50	<10	<2	0.16	5.8
62430	MM113-38-10	667945	5486574	100	0.5	1.8	0.07	59.0	362.35	14.52	<5	876	20.38	120.4	0.20	<10	2	0.62	39.0
62431	MM113-39-4	669304	5485670	42	<0.1	1.5	<0.01	4.1	55.70	3.05	<5	137	3.96	5.4	1.03	<10	<2	0.48	11.7
62432	MM113-39-11	670701	5485123	4949	<0.1	34.1	0.42	22.5	>10000.00	8.87	77	1421	5.88	36.3	7.20	<10	<2	1.50	38.1
62433	MM113-40-9	675337	5481491	70	1.3	0.2	0.16	15.9	38.68	4.08	24	996	3.46	3.8	4.90	<10	<2	0.67	70.9

porphyry. It is overlain by a felsic succession consisting of tuffs that are conformably overlain by rhyolite flows. Locally, the andesite unit pinches out and the felsic succession rests directly on basal conglomerate. East of Allison Creek the same general stratigraphy is recognized, however, the Spences Bridge Group rocks are locally strongly chlorite-epidote altered and can be difficult to distinguish from feldspar-phyric parts of the Nicola Group.

### 3.2.1. Conglomerate

Locally, the conglomerate consists of rounded granitic clasts, suggesting derivation mainly from the nearby Allison pluton. About 6 km west of Dry Lake, sparse granitic pebbles float in a grus-like matrix consisting of disaggregated crystals resembling those in the subjacent intrusion (Fig. 7a). Elsewhere, more diverse clast suites are exposed. For example, along the Allison Lake pluton margin southwest of Dry Lake on Highway 5A (Preto, 1979), and in the headwaters of Manning Creek, where conglomerate beds contain mainly volcanic and sedimentary clasts, with a large proportion derived from nearby Nicola Group (Fig. 7b). Intraformational conglomerate beds higher in the Spences Bridge Group section contain clasts from nearby Cretaceous and underlying Triassic strata and are indistinguishable from polymictic conglomerate beds at the base of the unit. Locally, well-bedded sandstone and siltstone interbeds form intervals up to a few metres thick. Rare exposures display cross stratification (Fig. 7c) and water escape structures. Tuff layers are common, with some composed exclusively of flattened dark green, chloritized pumice lapilli and coarse ash. A coarse sandstone to granulestone layer containing a few percent chloritized pumice lapilli was sampled for geochronological determination (sample MMI13-10-8, see Geochronology results, below). Near this locality, tongues of breccia along a rhyolite flow margin extend into conglomerate, demonstrating that felsic volcanism was coeval with coarse siliciclastic sedimentation.

### 3.2.2. Feldspar ± pyroxene andesite porphyry

Dark grey, feldspar-pyroxene-phyric andesites, interlayered with rhyolite breccia, occupy the lowest stratigraphic level east of Highway 5A. The andesite consists of fine to medium-grained plagioclase porphyry, with or without sparse pyroxene phenocrysts, in a dark green groundmass. It is mainly breccia, but also occurs as sparsely amygdaloidal flows. Epiclastic beds include several thin intervals of sandstone and intraformational volcanic conglomerate containing rounded clasts of fine-plagiophyric andesite, some as large as 40 cm in diameter.

The andesite porphyry unit generally lacks significant secondary alteration; this relatively fresh appearance distinguishes it from similar units in the Nicola Group in which epidote-chlorite-calcite extensively replaces groundmass and phenocrysts, and coats fractures.

### 3.2.3. Felsic tuff

The felsic tuff unit interfingers with, and ultimately overlies, the andesite unit. It contains a variety of light green and cream-colored, subangular and angular lithic pyroclasts typically smaller than a few centimetres diameter, but rarely attaining block size (Fig. 8a). In order of abundance, clasts include aphanitic and laminated rhyolite, fine-grained porphyritic

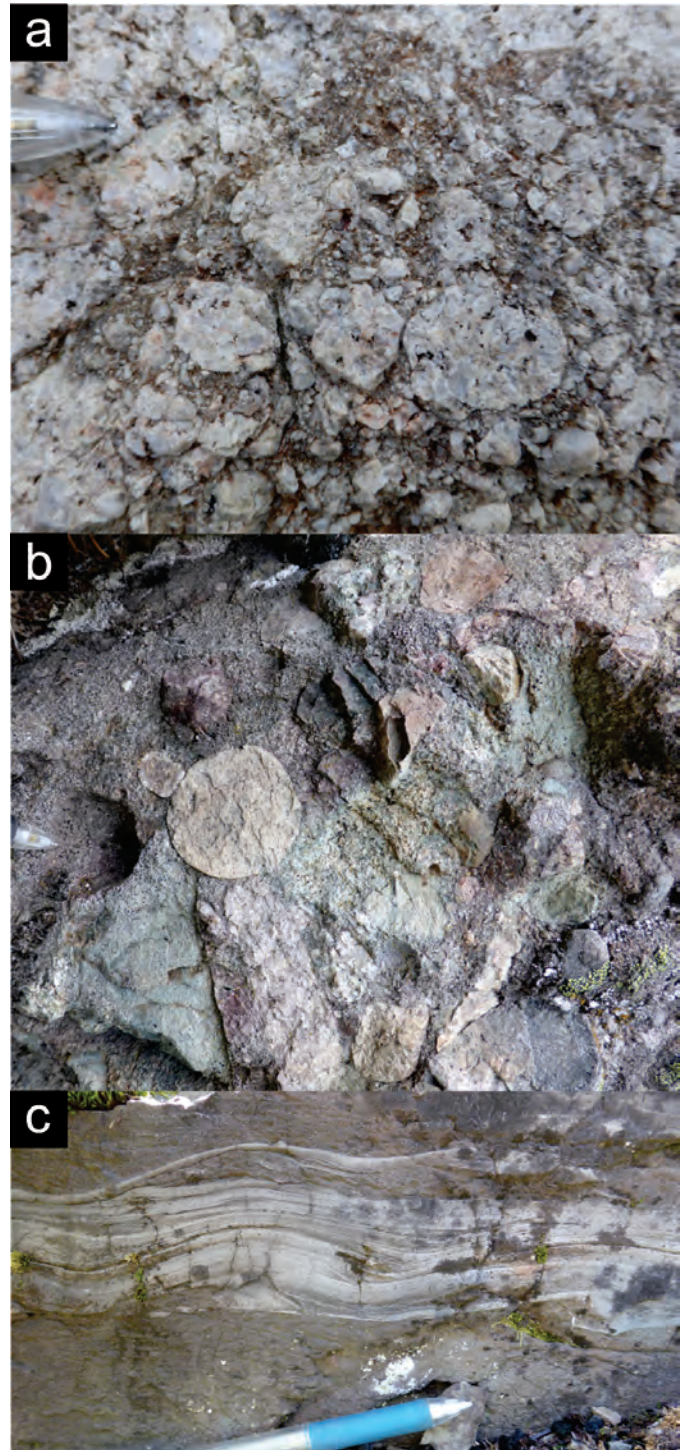


**Fig. 7.** Variation in Spences Bridge Group basal conglomerate ~6 km west of Dry Lake from **a**) grus-like granulestone with granitic fragments to **b**) polymictic containing clasts representing most units in the Nicola arc: augite porphyry (foliated and non-foliated), limestone, feldspar porphyry, Allison Lake granitoids, and diorite. **c**) Cross stratification in sandstone.

andesite, dark green chlorite-altered ash, and rare holocrystalline granitic lapilli. Plagioclase comprises up to 30 % of the matrix together with scattered quartz eyes. In several areas, fiamme define eutaxitic texture caused by welding (Fig. 8b), suggesting

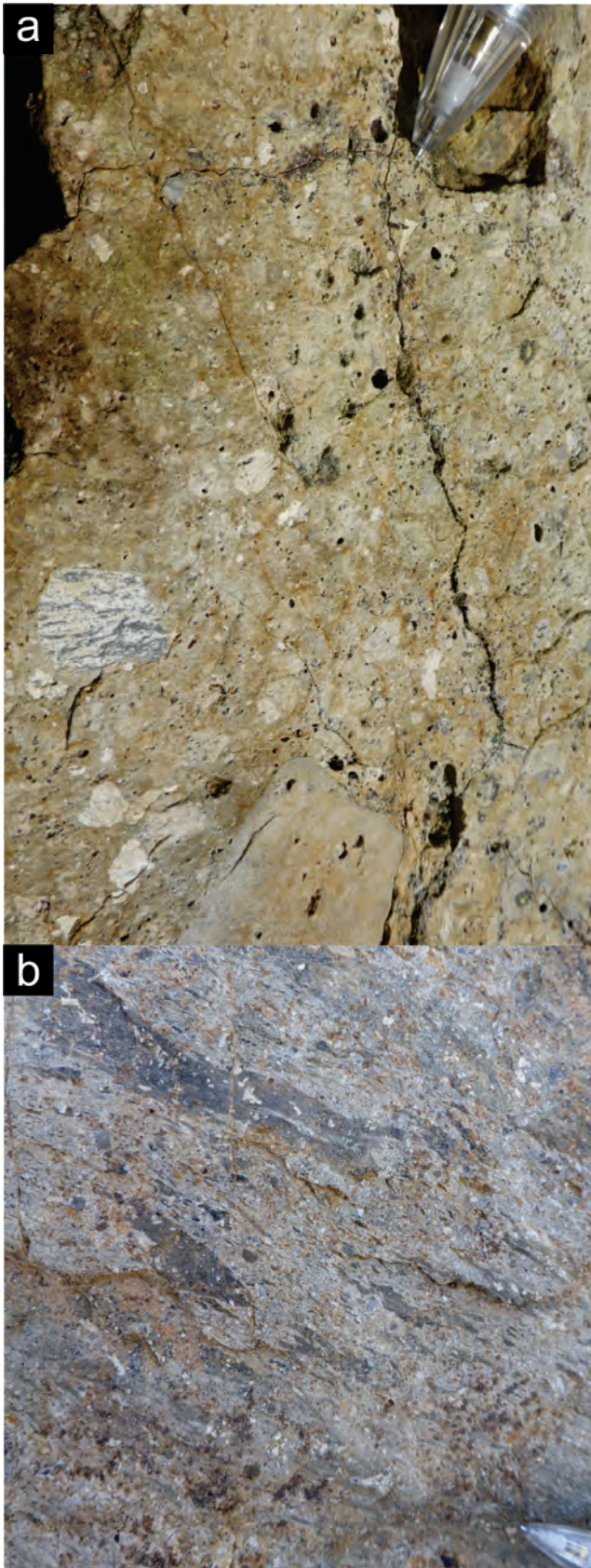


**Fig. 8.** Spences Bridge Group, Pimainus Formation. **a)** Felsic tuff showing characteristic aphanitic and flow-laminated rhyolitic fragments. **b)** Welded ignimbrite texture is locally developed.

that parts are ash-flow tuff deposits.

#### 3.2.4. Rhyolite flows

More than ~ 150 m of rhyolitic lava flows sharply overly the felsic tuff unit. West of Highway 5A (Allison Creek), they form resistant hummocks across an area greater than 13 km<sup>2</sup>. The flows appear homogeneous, showing only faint internal flow laminations. On fresh surfaces, they contain 15 to 20 percent medium-grained feldspar phenocrysts in a grey-green aphanitic groundmass. These formerly glassy rocks have devitrified to spherulites, and less commonly, small lithophysae, and alter to a chalky white, fine-grained assemblage composed mainly of clay minerals and quartz with hematite staining.

East of Highway 5A, rhyolite flows have a similar character but are more intimately interdigitated with other rock types, especially feldspar ± pyroxene porphyritic breccias and flows. In addition, the thickest, most massive rhyolite flows are cream to rusty white (like west of Allison Creek), but varicoloured, grey with white and pink flow-banded units are more numerous. Well-developed flow banding is characteristic, in addition to coarse flow breccia. Some individual flows are over 10 m thick.

The rhyolite deposits are probably flow domes and collapsed domes. However, coherent flows have been traced at least 500 m.

#### 3.2.5. Correlation

The provisional tripartite volcanic subdivision of the Spences Bridge Group in the study area broadly resembles the stratigraphy of the Pimainus Formation in the Shovelnose Mountain area, about 30 kilometres to the northwest as described by Diakow and Barrios (2009). Although lithofacies are similar at the Shovelnose section (> 2 km thick), they are thicker and recur at multiple levels. U-Pb zircon ages from samples taken near the base and the top of the Shovelnose Mountain constrain subaerial eruptions of the entire section to ~ 104 Ma (Thorkelson and Rouse, 1989; Diakow and Barrios, 2009). A U-Pb age determination from a rhyolite in the study area is pending; however, detrital zircons from a coarse sandstone immediately adjacent to flow-banded rhyolite, yielded a cluster of ages around 103 Ma, suggesting derivation from the rhyolite and coeval tuff (see Geochronology below).

### 3.3. Princeton Group

Eocene rocks of the Princeton Group have long been a target for coal exploration, hence Princeton Basin has been relatively well mapped (see synthesis by McMechan, 1983). We mapped a ~ 3 km<sup>2</sup> area of Princeton Group along the eastern margin of Princeton Basin, near the Boundary fault north of Miner Mountain, and a ~ 1 km<sup>2</sup> area near Rampart Lake (Fig. 3).

#### 3.3.1. Rhyolite breccia

Mauve to tan, flow-banded rhyolite breccia discontinuously in a clearcut ~ 4 km north-northeast of Rampart Lake (Mihalynuk and Logan, 2013b). Although the basal contact is not exposed, we infer that the breccia was deposited unconformably above Late Triassic Nicola Group augite porphyry volcanic rocks and an outlier of the Summers Creek pluton.

Mihalynuk and Logan (2013b) included these rocks with the Spences Bridge Group (Early Cretaceous), the closest previously mapped felsic volcanic rocks (Monger, 1989).

However, the rocks are similar to volcanic units in the Princeton Group as described by (Church, 1973). To resolve this ambiguity we collected a sample for geochronological study. Based on lithology and an  $^{40}\text{Ar}/^{39}\text{Ar}$  plateau age of  $50.2 \pm 0.6$  Ma (see Geochronology below), we now correlate the breccia with volcanic rocks of the Princeton Group described by McMechan (1983).

### 3.3.2. Rhyolite ash tuffite and arkose

Recessive weathering, white arkosic wacke to granulestone (Fig. 9a) contain coal partings and uniform ash layers up to several centimetres thick. Ash layers are distinguished by their low density and black vitric shards that stand out in sharp contrast to the white, clay-rich matrix. Cusped margins on the shards (Fig. 9b) distinguish them from coal fragments. The partings and fragments of coal in the sandstones and granulestones suggest sedimentation in a fluvial setting that was intermittently blanketed by pyroclastic material.

This unit correlates with Allenby Formation unit 7e of McMechan (1983). The Allenby Formation was assigned a middle Eocene age based on fossil teeth from *Trogosus*, a bear-

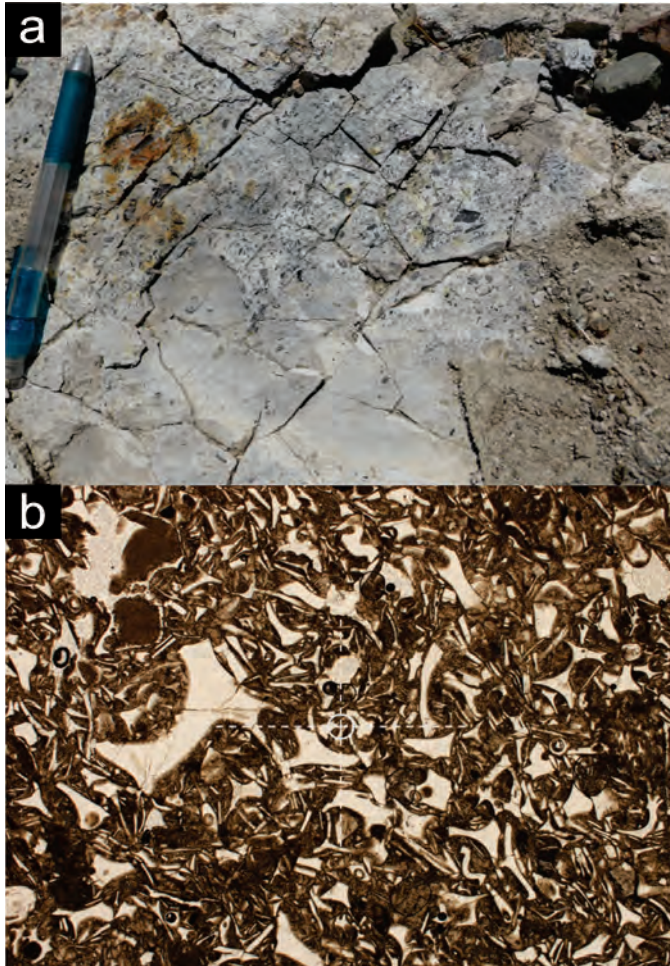


**Fig. 9.** Princeton Group rhyolite ash tuffite and arkose unit. **a)** Tuffaceous sandstone and granulestone with some layers containing abundant black coaly material. **b)** Photomicrograph of tuff layer with angular, concavo-convex shards (plane polarized light, field of view is  $\sim 4$  mm).

like rodent (Russell, 1935). However, a U-Pb age of  $52.08 \pm 0.12$  Ma (Mortensen and Archibald, in Moss et al., 2005) from tuff layers at an Allenby fossil flora site indicate that part of the unit is no younger than early Eocene. Ickert et al. (2009) collated available isotopic ages to show that Princeton Group magmatism lasted from 53 to 47 Ma (early part of Eocene, Cohen et al., 2013 timescale).

### 3.3.3. Osprey pebble-bearing conglomerate

Exposures of Princeton Group strata north of Miner Mountain are predominantly granule to cobble conglomerate and immature sandstone. Most conglomerate beds contain mainly K-feldspar crystal and granite clasts (Fig. 10a) almost certainly derived from the Osprey batholith, 7 km to the northeast (McMechan, 1983; Hills, 1965), consistent with southwest paleocurrents (McMechan, 1983).

A curious feature of the Osprey pebble conglomerate near Miner Mountain is that many clasts are broken, as seen upon microscopic examination (Fig. 10b). Clast fragments have been

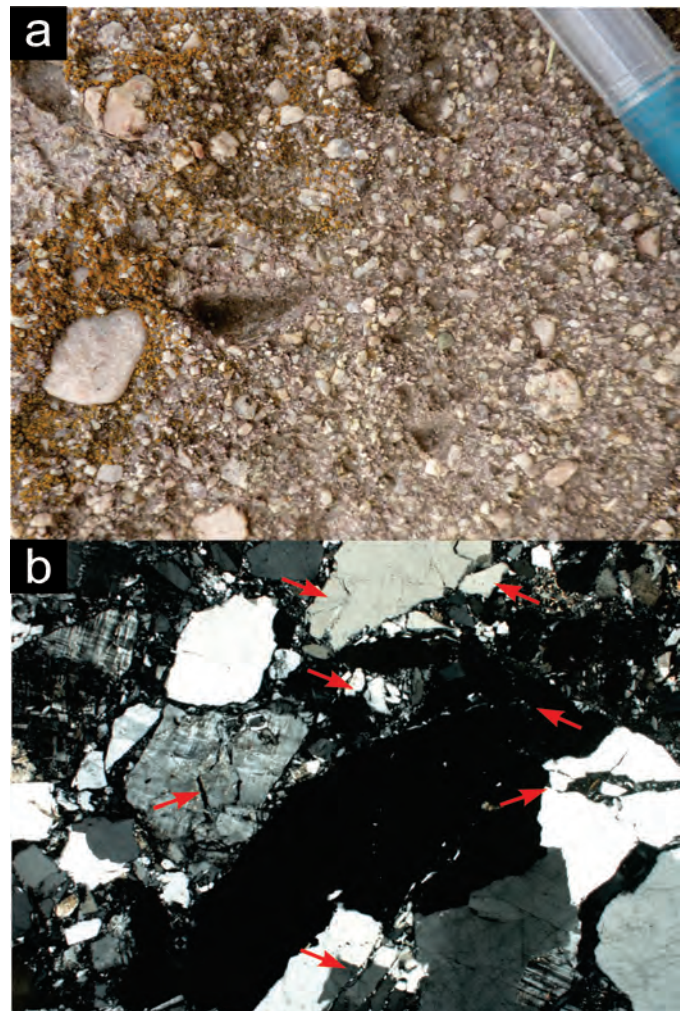


**Fig. 10.** Princeton Group, Osprey pebble-bearing conglomerate unit. **a)** Pebble and granule conglomerate derived primarily from the Osprey Lake batholith. **b)** Photomicrograph of conglomerate shows quartz and feldspar grains have been broken (arrows), fragments translated and rotated, and fractures infilled with matrix material (crossed polarized light, field of view is  $\sim 4$  mm).

variably rotated and the spaces between infilled with matrix material. The process responsible for grain fragmentation is speculative, but it may be related to extensional faulting. If so, it is of importance to ongoing porphyry copper exploration at Miner Mountain.

### 3.4. Chilcotin Group

Outliers of Cenozoic olivine basalt of the Chilcotin Group (Mathews, 1989), crop out sporadically at elevations between 1240 and 1620 asl. The basalts unconformably overlie the Spences Bridge rhyolite flow unit. Dry exposures are dun to orange weathering with darker brown spots identifying small, less than 2 millimetre diameter, olivine grains. Fresh surfaces are jet-black and shimmer in sunlight due to the fresh, fine-crystalline aggregate of plagioclase microlites and 15 to 20 percent yellowish olivine grains (Fig. 11). Deeply-weathered exposures display bulbous, onion skin exfoliation concentrated along fractures, and dark green-grey or brown fresh surfaces. Brownish soil results from weathering of the basalt and is a telltale indicator where it is concealed by thin overburden. Massive, locally columnar jointed flows can form uninterrupted cliff faces more than 8 m high. At one locality, olivine basalt sharply overlies oxidized deep red to purple scoria and amygdaloidal basalt, with the amygdales infilled by oxidized, chalky zeolite (?) and white chalcedony. A suite of weathered dikes exposed along the Tulameen River are interpreted as correlative. They are cut and offset by shallowly dipping faults.



**Fig. 11.** Contrasting dun-weathering and jet black fresh surfaces of Miocene Chilcotin Group plateau basalt.

Flows overlying the Eocene coal measures near Coalmont have K-Ar ages of 9 and  $9.2 \pm 1.8$  Ma (Mathews, 1989; Breitsprecher and Mortensen, 2004; Late Miocene, Cohen et al., 2013 timescale).

### 4. Intrusive units

Plutonic rocks in the study area range from Late Triassic to Eocene (Fig. 3) and dikes are as young as those interpreted to feed the Chilcotin Group. The eastern parts of the study area are underlain by the southern limits of the Pennask batholith ( $194 \pm 1$  Ma; Early Jurassic) and western parts of the Bromley pluton (193 Ma), both of which are cut by the Osprey Lake K-feldspar megacrystic granite batholith ( $166 \pm 1$  Ma; U-Pb zircon, Parrish and Monger, 1992). In the central belt, as defined by Preto (1979), Late Triassic intrusions mark the axis of the Nicola arc and include the Allison Pluton ( $204 \pm 10$  to  $207 \pm 10$  Ma, K-Ar hornblende and muscovite cooling ages in Preto, 1979; recalculated by Breitsprecher and Mortensen, 2004) and numerous undated dioritic bodies interpreted as part of the  $\sim 205$  Ma Copper Mountain suite. Also along the arc axis is the Summers Creek stock (middle Cretaceous,  $99.1 \pm 1$  to  $101 \pm 5.2$  Ma, K-Ar biotite, Preto, 1979; recalculated by Breitsprecher and Mortensen, 2004), which may be comagmatic with the Spences Bridge Group. Along the western margin of the study area is the Boulder intrusion. Although undated, it is presumed to be Jurassic because it intrudes Nicola Group, and is in turn cut by the Otter Lake stock (Cretaceous; Massey and Oliver, 2010). Outcrops of the Pennask batholith were not encountered in the map area. For descriptions of the Osprey and Copper Mountain intrusions see Mihalynuk and Logan (2013a, b). Probable Copper Mountain suite equivalents are described in Mineralization section below. Possible hypabyssal equivalents to the Summers Creek pluton are the Mine dikes (also known as Candy Stripe dikes), are also described in Mihalynuk and Logan (2013a). Similar north-trending dikes are common in the study area.

#### 4.1. Allison Lake pluton

The Allison Lake pluton underlies an area of  $\sim 160$  km<sup>2</sup> in the northern part of the study area. It cuts Late Triassic Nicola Group in the east, and is nonconformably overlain by basal strata of the Spences Bridge Group. The Allison fault has an inferred sinistral offset within the pluton; it continues outside, trending farther northwest where the fault juxtaposes an elongate plutonic body against Cretaceous and Eocene strata (Monger, 1989; note that a colouring error on this map shows Nicola Group breccia east of Allison Lake, where it is meant to show pluton).

Preto (1979) subdivided the pluton into main granite to monzonite phases and subordinate granodiorite to gabbro phases. Outcrops at valley level, southwest of Dry Lake along Highway 5A, expose reddish, medium-grained, equigranular granite or quartz monzonite containing 25 percent (combined) hornblende and biotite. The pluton contains irregular sheared, rusty aphanitic mafic volcanic xenoliths, similar to rocks considered to be Nicola Group bordering the pluton. Rocks in the contact zone are locally malachite stained. Farther west on the plateau, variegated tonalitic and granodioritic phases occur near the margin of the pluton. At two localities along the margin, the intrusion consists of  $> 2$  m wide zones of frothy

quartz and matted tourmaline in veinlets.

#### 4.2. Bromley pluton

Bromley pluton is a typical white to pink-weathering granodiorite. In the study area, its contact follows Hayes Creek where it has intruded and thermally metamorphosed the Nicola Group, upgrading adjacent rocks to biotite grade within about 500 metres of the contact, and biotite-garnet within a few tens of metres of the contact. The pluton contains conspicuous books of euhedral biotite 0.5 cm across and 1 cm thick that comprise ~ 5% of the rock. Hornblende comprises ~ 10%, and together with biotite, is variably chloritized.

Subparallel with the contact is an extensive set of dikes, typically containing phenocrysts of K-feldspar, plagioclase, quartz, and chloritized hornblende in varying combinations. Some dikes attain widths of 10 m or more. They are interpreted to be co-genetic with the Bromley pluton; however, a preliminary U-Pb zircon determination suggests that one of the widest dikes is middle Cretaceous, correlative with the “Mine dikes” and Spences Bridge Group.

#### 4.3. Boulder intrusion

The Boulder intrusion is compositionally variable, with major phases of quartz diorite to granodiorite. Outcrops are invariably cut by parallel sets of epidote-chlorite  $\pm$ pyrite-quartz-calcite veinlets (Fig. 12). Many of these veinlets have a white or pinkish halo interpreted as secondary alkali feldspar that extends a centimetre or more from the vein wall. Some intrusive phases display conspicuous miarolitic cavities up to 0.5 cm across; these phases tend to be more quartz-rich.

Near its western contact, a strongly cataclastic fabric is locally developed. Near its southern termination, it is very pyritic with overlying metres-thick gossanous zones of Fe-oxide/hydroxide-cemented colluvium.

#### 4.4. Summers Creek pluton

Many outcrops of the Summers Creek pluton are granodioritic and display characteristic crowded medium- to coarse-grained, blocky plagioclase crystals and prismatic hornblende. Interstices between large grains are filled by late K-feldspar-quartz, fine-grained biotite-hornblende and ~ 1% magnetite. Mafic xenoliths are common (~ 0.5%) and only partly digested, suggesting high-level stopping. A sample was collected for U-Pb age determination to confirm three middle Cretaceous K-Ar age determinations (Preto, 1979); results are pending.

### 5. Structure

Folding and faulting have both played a role in the distribution and orientation of rock packages across the study area, but the contribution of each throughout time is difficult to assess, especially in the central and eastern belts. Part of the difficulty arises from the superposition of different faulting events. In general, earliest syndepositional basin-forming faults have been overprinted by strike-slip faults, and further modified during episodes of late extensional faulting. Extensive dissection of folds by later faulting obscures the original cause of bedding orientation changes. Folds that are most susceptible to such overprinting are intermediate in scale: regional fold patterns will persist despite local faults, and outcrop-scale folds will persist between fault strands, but folds



**Fig. 12.** Boulder intrusion displays intergrown fresh grey plagioclase that becomes turbid and weathers white to pink- where altered along epidote-lined fractures. An incipient fracture is located at the 0.5mm pencil tip and an epidote-lined fracture is along the left side of the photo.

with wavelengths of hundreds of metres are most likely to lose coherence through fault dissection. Thus, we recognize a gentle regional synform east of northern Summers Creek (Mihalynuk and Logan, 2013b), and can point to outcrop-scale folds (Fig. 13a) with half wavelengths of up to ~ 100 m, but well-documented intermediate-scale folds are lacking. Existence of such folds and repetition by thrust faults can be verified in areas with excellent exposure and easily traced marker units, such as at Hedley to the immediate east (Ray and Dawson, 1994) and along the Coquihalla Highway to the northwest (Diakow and Barrios, 2008).

Systematic changes in bedding-phyllitic cleavage relationships in western Nicola Group sedimentary rocks document intermediate-scale folding. Intensity of folding increases westward into the Eagle Metamorphic complex (Massey and Oliver, 2010), which was deformed in the Late Jurassic and Middle Cretaceous (Greig et al., 1992).

### 6. Faults

Regional, possibly long-lived, steep faults were recognized by Preto (1979) and Monger (1989) along Summers and Allison creeks, the Tulameen River west of Coalmont, and bounding the Princeton Basin.

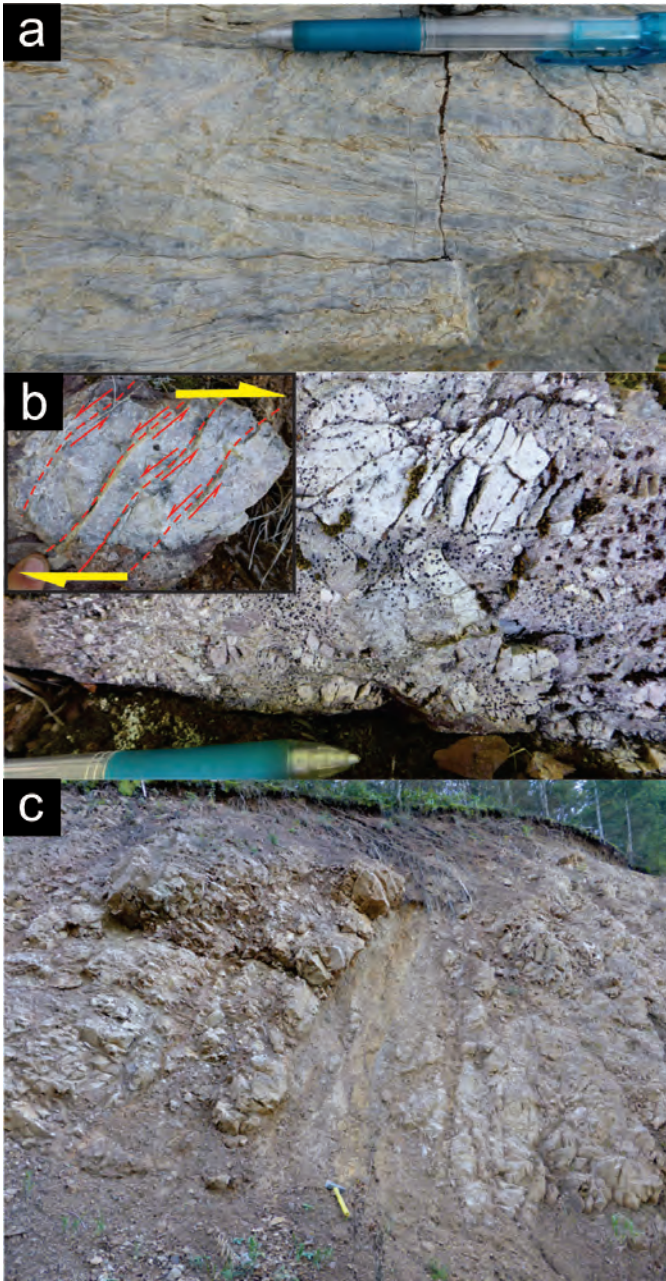


**Fig. 13.** a) Carbonate tectonite displays intrafolial isoclinal folds. b) Calcareous volcanic sandstone deforms in a ductile fashion around brittle blocks with antithetic sinistral faults, consistent with an overall dextral sense of shear. c) One of a set of brittle fault gouge zones parallel to the main trace of the Allison Creek fault in the upper Allison Creek valley; here the faults cut volcanic rocks interpreted as Spences Bridge Group.

### 6.1. Summers Creek and Allison Creek faults

Summers Creek and Allison Creek faults are part of a north-northwest-trending system that extends for at least 160 km and is suspected to have focused emplacement of mineralized Late Triassic plutons (Preto, 1979). On its western boundary, the Summers Creek fault system passes into a zone of ductile strain. Cored drill intercepts of this zone at the Axe deposit reveal carbonate clasts with elongation ratios between 10 to 20 (extend beyond core diameter). North of the Axe, the zone is at

least 300m wide and involves quartz-sericite-altered felsic tuff and carbonate. Foliation developed in the carbonate is locally strongly folded; axial surfaces dip from steeply southeast to nearly horizontal (Fig. 13 a) and hinges plunge 35-45° northeast. Late stages of motion generated voids along minor fabric-parallel faults and perpendicular carbonate-filled extensional veins. A dextral sense of shear is indicated by semi-rigid blocks that are cut by antithetic brittle faults in a more ductile, finer-grained, carbonate-rich matrix (Fig. 13b). A sample of rhyolite from the strain zone was collected to establish the maximum age of deformation.

Near Summit Lake, the Allison Creek fault appears to have juxtaposed Spences Bridge Group against the Allison pluton. Within ~ 0.5 km west of Allison Creek, numerous discrete faults that cut the adjacent Spences Bridge Group mainly dip moderately to steeply east (Fig. 13c).

### 6.2. Extensional faults

Down-to-the-west extensional faults (as indicated by fault corrugations, steps, and slickensides) are well exposed along the Old Hedley Road where they offset a pegmatitic sill (Fig. 14a) cutting Nicola Group volcano-sedimentary strata that are thermally metamorphosed to biotite grade. In most places the faults clearly cut the pegmatitic sill, but at one locality the sill is cut by, and then cross-cuts a shallow fault plate (Fig. 14b). We interpret this as evidence of syn-extensional intrusion. A sample of the pegmatite was collected to establish the age of deformation.

Low-angle faults also offset dikes along the Coalmont Road between Coalmont and Princeton. Based on the rotation of hangingwall and footwall fabrics, the apparent sense of offset is top-to-the-west, but the fault zone is shattered and the dikes are friable (Fig. 14c), so a reliable fault lineation could not be evaluated. Nevertheless, the offset dikes are interpreted as feeders to overlying Chilcotin plateau basalt. If correct, extensional deformation may range to at least as young as Miocene.

## 7. Geochronology

Geochronological results for all but one of the 16 samples collected in 2013 are pending. Presented here are completed analyses from samples collected during 2012 fieldwork, which focused on areas around the Miner Mountain deposit and the Primer South prospect.

### 7.1. Methods

#### 7.1.1. Hornblende and biotite $^{40}\text{Ar}/^{39}\text{Ar}$ : Laser step heating

Samples were crushed in a ring mill, washed in distilled water and ethanol, and sieved when dry to - 40 + 60 mesh. Biotite or hornblende were then picked out of the bulk fraction, wrapped in aluminum foil and stacked in an irradiation capsule into which samples of similar ages and neutron flux monitors (Fish Canyon Tuff sanidine (FCs),  $28.201 \pm 0.046$  Ma, Kuiper et al., 2008) were added. Sample irradiation at the McMaster Nuclear Reactor in Hamilton, Ontario, occurred for 180 MWH in the medium flux site 8E. Analyses ( $n=65$ ) of 17 neutron flux monitor positions produced errors of < 0.5% in the J value.

Sample analyses were conducted at the Noble Gas Laboratory, Pacific Centre for Isotopic and Geochemical Research (PCGIR), University of British Columbia, Vancouver, BC, Canada. The

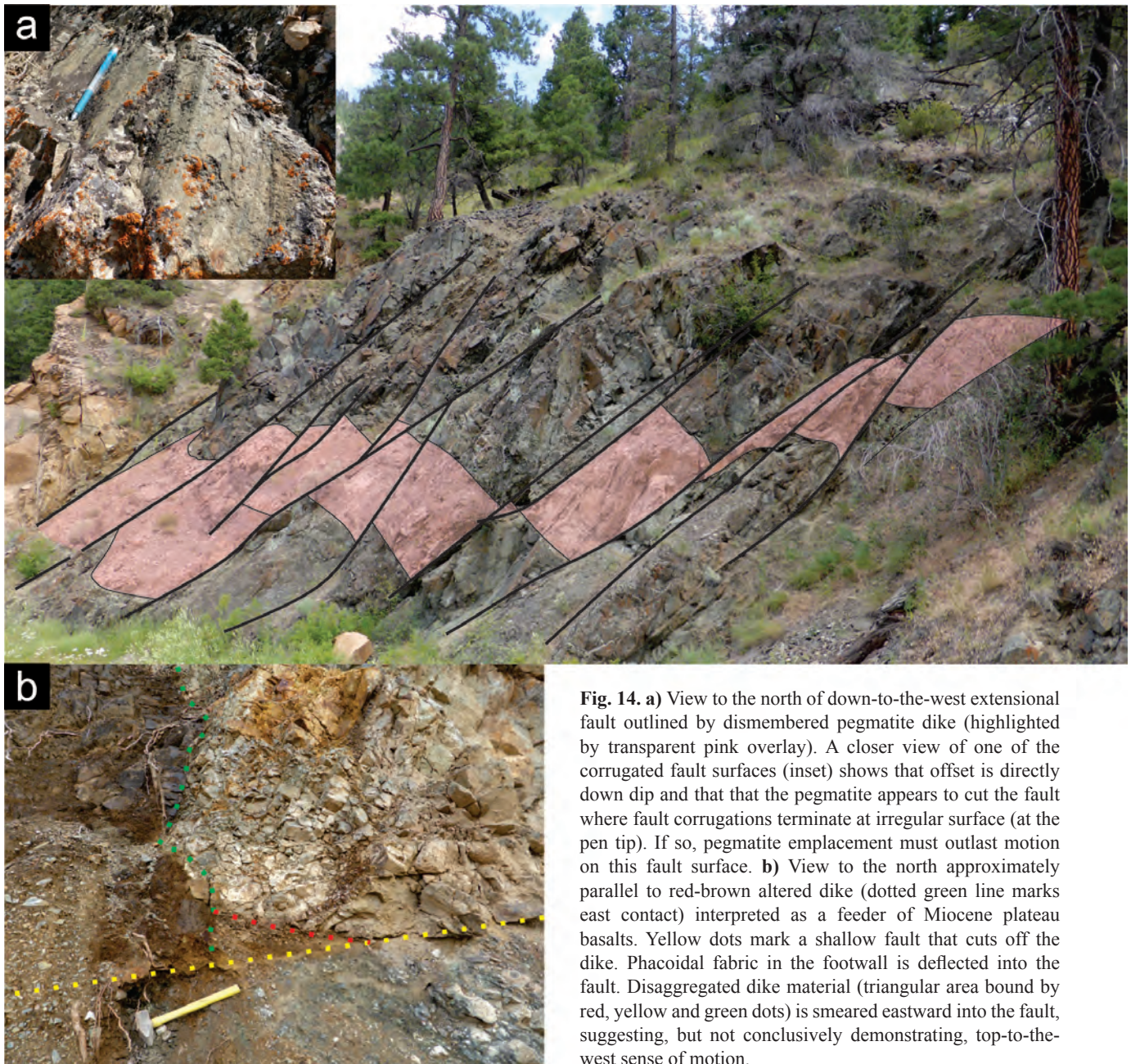


**Fig. 14. a)** View to the north of down-to-the-west extensional fault outlined by dismembered pegmatite dike (highlighted by transparent pink overlay). A closer view of one of the corrugated fault surfaces (inset) shows that offset is directly down dip and that the pegmatite appears to cut the fault where fault corrugations terminate at irregular surface (at the pen tip). If so, pegmatite emplacement must outlast motion on this fault surface. **b)** View to the north approximately parallel to red-brown altered dike (dotted green line marks east contact) interpreted as a feeder of Miocene plateau basalts. Yellow dots mark a shallow fault that cuts off the dike. Phacoidal fabric in the footwall is deflected into the fault. Disaggregated dike material (triangular area bound by red, yellow and green dots) is smeared eastward into the fault, suggesting, but not conclusively demonstrating, top-to-the-west sense of motion.

mineral separates were step-heated at incrementally higher powers in the defocused beam of a 10W CO<sub>2</sub> laser (New Wave Research MIR10) until fused. Gas evolved from each step were analyzed by a VG5400 mass spectrometer equipped with an ion-counting electron multiplier. All measurements were corrected for total system blank, mass spectrometer sensitivity, mass discrimination, and radioactive decay during and subsequent to irradiation, and interfering Ar from atmospheric contamination and the irradiation of Ca, Cl, and K using isotope production ratios of:  $(^{40}\text{Ar}/^{39}\text{Ar})\text{K} = 0.0302 \pm 0.00006$ ,  $(^{37}\text{Ar}/^{39}\text{Ar})\text{Ca} = 1416.4 \pm 0.5$ ,  $(^{36}\text{Ar}/^{39}\text{Ar})\text{Ca} = 0.3952 \pm 0.0004$ ,  $\text{Ca}/\text{K} = 1.83 \pm 0.01(^{37}\text{ArCa}/^{39}\text{ArK})$ .

Initial data entry and calculations were performed using ArArCalc algorithms (Koppers, 2002). Plateau and correlation

ages were calculated using Isoplot ver.3.09 (Ludwig, 2003). Errors were propagated from all sources except mass spectrometer sensitivity and age of the flux monitor at the  $2\sigma$  (95% confidence) level. A plateau age was calculated from the statistical best fit where: 1) more than 60% of the <sup>39</sup>Ar comprised three or more contiguous steps; 2) the probability of fit of the weighted mean age was greater than 5%; 3) the slope of the error-weighted line through the plateau ages equaled zero at 5% confidence; 4) the ages of the two outermost steps on a plateau were not significantly different from the weighted-mean plateau age (at  $1.8\sigma$ , six or more steps only); the outermost two steps on either side of a plateau did not have nonzero slopes with the same sign (at  $1.8\sigma$ , nine or more steps only).

### 7.1.2. Zircon: Chemical Abrasion - Thermal Ionization Mass Spectroscopy (CA-TIMS)

CA-TIMS procedures described here are modified from Mundil et al. (2004), Mattinson, (2005) and Scoates and Friedman (2008). Rock samples underwent standard mineral separation procedures; zircons separates were handpicked in alcohol. The clearest, crack- and inclusion-free grains were selected, photographed and then annealed at 900°C for 60 hours. Annealed grains were chemically abraded and then spiked with a  $^{233-235}\text{U}$ - $^{205}\text{Pb}$  tracer solution (EARTHTIME ET535), and then dissolved. Resulting solutions were dried and loaded onto Re filaments (Gerstenberger and Haase, 1997).

Isotopic ratios were measured by a modified single collector VG-54R or 354S thermal ionization mass spectrometer equipped with analogue Daly photomultipliers. Analytical blanks are 0.2 pg for U and 1.0 pg for Pb. U fractionation was determined directly on individual runs using the ET535 mixed  $^{233-235}\text{U}$ - $^{205}\text{Pb}$  isotopic tracer. Pb isotopic ratios were corrected for fractionation of 0.23%/amu, based on replicate analyses of NBS-982 reference material and the values recommended by Thirlwall (2000). Data reduction employed the Excel™-based program of Schmitz and Schoene (2007). Standard concordia diagrams were constructed and regression intercepts, weighted averages calculated with Isoplot (Ludwig, 2003). All errors are quoted at the 2 $\sigma$  or 95% level of confidence, unless otherwise noted. Isotopic dates are calculated with the decay constants  $\lambda^{238}=1.55125\text{E-}10$  and  $\lambda^{235}=9.8485\text{E-}10$  (Jaffe et al., 1971). EARTHTIME U-Pb synthetic solutions were analysed on an on-going basis to monitor the accuracy of results.

### 7.1.3. Zircon: Laser Ablation (LA) ICP-MS

Zircons analyzed using laser ablation (LA) ICP-MS employ techniques as described by Tafti et al. (2009). Instrumentation at the PCIGR comprises a New Wave UP-213 laser ablation system and a ThermoFinnigan Element2 single collector, double-focusing, magnetic sector ICP-MS. All zircons greater than about 50 microns in diameter were picked from the mineral separates and mounted in an epoxy puck along with several grains of the Plešovice ( $337.13 \pm 0.13$  Ma, Sláma et al., 2007), and Temora2 ( $416.78 \pm 0.33$  Ma) zircon standards and brought to a very high polish. Prior to analysis, the surface of the mount was washed for 10 minutes with dilute nitric acid and rinsed in ultraclean water. The highest quality portions of each grain selected for analysis were free of alteration, inclusions, or possible inherited cores. Line scans rather than spot analyses were employed to minimize elemental fractionation during the analyses. A laser power level of 40% and a 25  $\mu\text{m}$  spot size were used. Backgrounds were measured with the laser shutter closed for ten seconds, followed by data collection with the laser firing for approximately 35 seconds. The time-integrated signals were analysed using Iolite software (Patton et al., 2011), which automatically subtracted background measurements, propagated all analytical errors, and calculated isotopic ratios and ages. Corrections for mass and elemental fractionation were made by bracketing analyses of unknown grains with replicate analyses of the Plešovice zircon standard. A typical analytical session at the PCIGR consists of four analyses of the Plešovice standard zircon, followed by two analyses of the Temora2 zircon standard five analyses of unknown zircons, two standard analyses, five unknown analyses, etc., and finally two Temora2

zircon standards and four Plešovice standard analyses. The Temora2 zircon standard was analysed as an unknown to monitor the reproducibility of the age determinations on a run-to-run basis. Final interpretation and plotting of the analytical results employed the ISOPLOT software of Ludwig (2003).

## 7.2. Geochronology results

Complete raw data tables, cathode luminescence imagery of zircons analyzed, and ancillary plots such as inverse  $^{40}\text{Ar}/^{39}\text{Ar}$  isochrons and Ca/K can be found in Mihalynuk et al. (2014b).

### 7.2.1. Hornblende and biotite $^{40}\text{Ar}/^{39}\text{Ar}$

Release spectra and interpreted ages for three samples are presented in Figure 15 (a, b, c) and the data are presented in Table 2.

Sample MMI12-5-8 (Fig. 15a) was collected from a mineralized hornblende diorite at the Primer South prospect (see Mihalynuk and Logan 2013b, c for description and major and minor element geochemistry). A good plateau, formed by six steps, includes 98.7% of the  $^{39}\text{Ar}$  released. There is no obvious sign of thermal disturbance and the sample analyzed is relatively fresh and unlikely to have been completely reset. Thus, the plateau age,  $188.2 \pm 2.5$  Ma is interpreted as recording the post eruptive crystallization age.

Mihalynuk and Logan (2013b) and previous workers assumed that the intrusion was part of the Copper Mountain suite (~ 205-200 Ma, Late Triassic). However, the new age, if interpreted correctly, requires emplacement in the Early Jurassic. Intrusions of this age are known elsewhere in the Nicola arc. For example, to the north, young, mainly mafic phases of the Takomkane batholith have ages of  $187.7 \pm 1.1$  Ma ( $^{40}\text{Ar}/^{39}\text{Ar}$  hornblende (Schiarrizza et al., 2009), and in southern BC, the Bromley batholith has a K/Ar hornblende cooling age of  $186 \pm 3$  Ma (Hunt and Roddick, 1988), and the Skwel Peken Formation age is ~  $187 \pm 9$  Ma based on 3 discordant zircon fractions (Ray and Dawson, 1994).

Sample MMI12-8-6 (Fig. 15b) was collected from a hornblende-pyroxene porphyritic volcanic breccia that interrupts a thick epiclastic succession (Mihalynuk and Logan, 2013b) upsection from augite porphyry breccias and flows that are the defining rock types of the Nicola arc. Fresh euhedral hornblende from this unit yields a stable plateau with 94.3% of  $^{39}\text{Ar}$  released in 9 of 11 steps from which an age of  $182.1 \pm 2.3$  Ma is calculated (first and last steps omitted from age calculation).

The hornblende lacks a fabric and is unaltered (see Fig. 6 of Mihalynuk and Logan, 2013b) suggesting that the sample has not been completely reset. Therefore, we interpret that the age records crystallization at the time of eruption. In addition, intercalation of this unit with epiclastic strata, which contain clasts lithologically identical to dated pluton sample MMI12-5-8, is consistent with an age younger than ~ 188 Ma. Early Jurassic magmatic ages such as these are important in southern Quesnellia as they show that Nicola arc volcanism extended into the Early Jurassic, and is not limited to the Late Triassic as has been widely assumed.

Sample MMI12-7-4 (Fig. 15c) was collected near the northern boundary of the 2013 study area, from an oxyhornblende-pyritic rhyolite breccia (see section 3.3.1 above) interpreted as part of a series of coalescing flow domes (Mihalynuk and

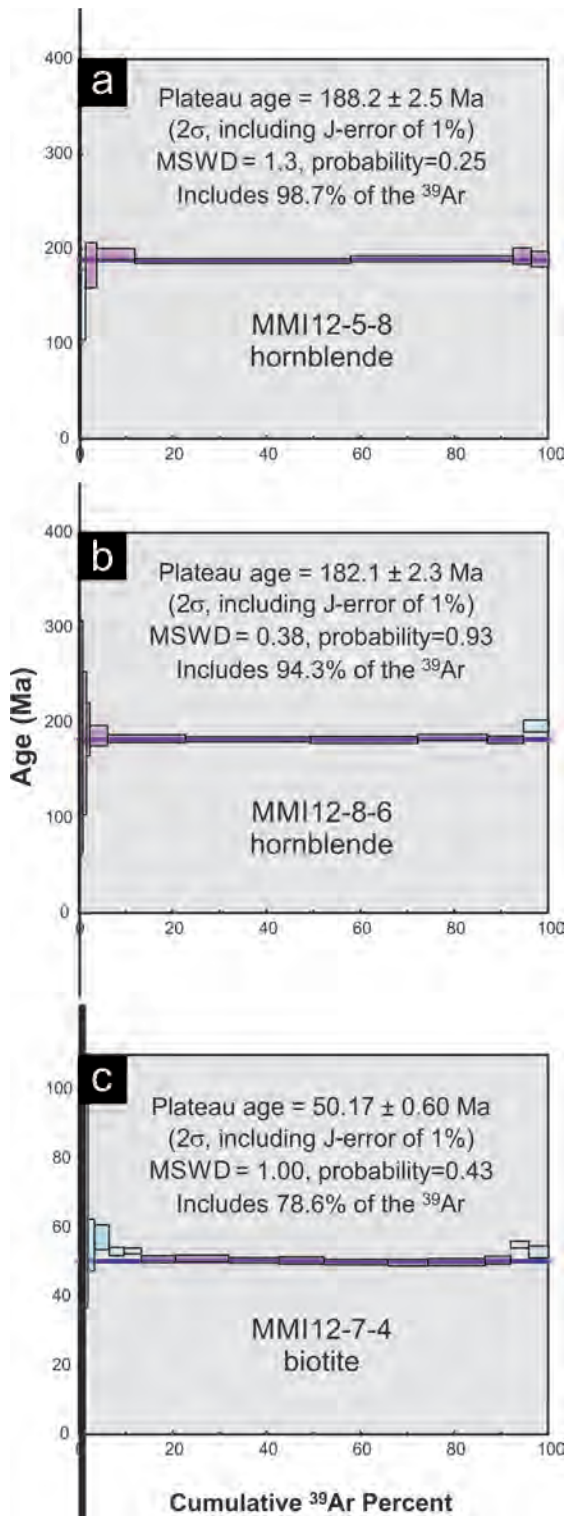


**Fig. 15.** Argon release spectra yield  $^{40}\text{Ar}/^{39}\text{Ar}$  cooling ages from the Dillard Creek area. **a)** Sample MMI12-5-8 is from mineralized diorite at the Primer deposit. **b)** MMI12-8-6 is from hornblende-pyroxene porphyry lapilli tuff and breccia that presumably caps the Primer section. **c)** MMI12-7-4 is from a section of rhyolite flows, breccia and tuff south of the Primer, originally suspected to correlate with the Early Cretaceous Spences Bridge Group, but based on its age, fits well with the Princeton Group. Plateau steps are shown in magenta, rejected steps are cyan. Box heights are  $2\sigma$ .

Logan, 2013b). A release spectrum with a strong plateau comprising 78.6% of the  $^{39}\text{Ar}$  yields a calculated age of  $50.2 \pm 0.6$  Ma. Previously considered part of the Spences Bridge Group (Mihalynuk and Logan, 2013b), this new age indicates that it is part of the Princeton Group. The Early Eocene, 50 Ma age is typical of the late stage of Eocene magmatism that swept across southern British Columbia (Bordet et al., 2013).

### 7.2.2. U-Pb CA-TIMS and LA-ICPMS

Concordia plots for two samples are presented in Figures 16a and 16a and corresponding data are presented in Tables 3 and 4. Age distribution of individual zircons analyzed by LA-ICPMS is presented in Figure 17b.

Sample MMI12-3-15 was collected in the Southwest zone at Miner Mountain from a rusty diorite dike that contains chalcopyrite as disseminations and veins. Descriptions of the dike, its major and trace element geochemistry, and mineralization are presented in Mihalynuk and Logan (2013a). Five single zircon grains were analyzed: three whole crystals, which were anhedral, oblate, pitted, and up to  $\sim 200$   $\mu\text{m}$  long; and two crystal fragments about  $\sim 100$   $\mu\text{m}$  and  $\sim 70$   $\mu\text{m}$  in

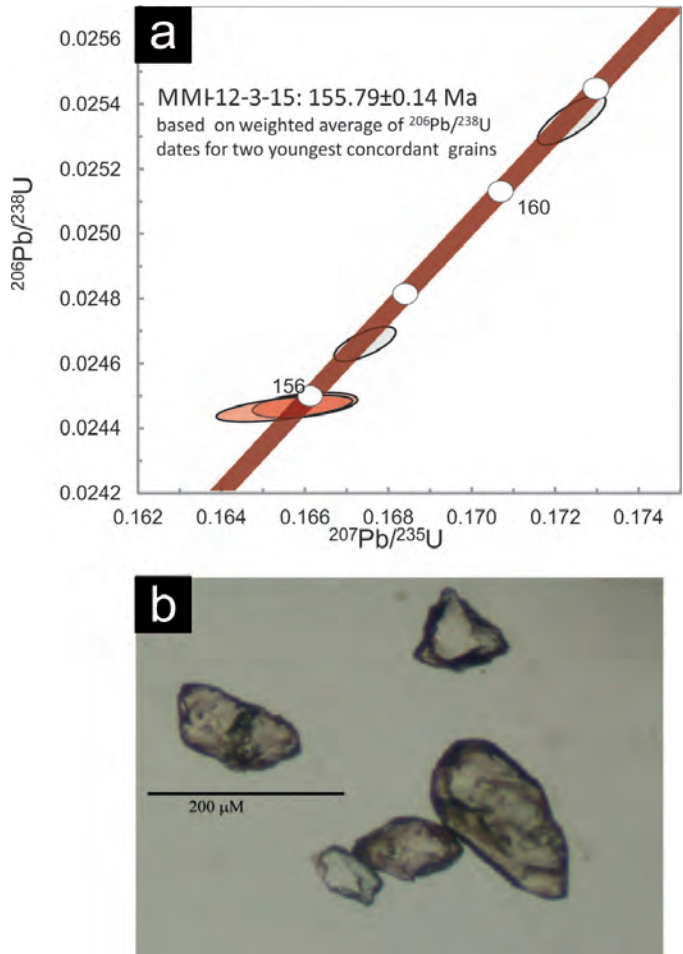


**Fig. 16. a)** Thermal Ionization Mass Spectrometric (TIMS) analysis of zircon U-Pb from a sample of mineralized dyke at the Southwest zone on Miner Mountain. Best estimate of the age is  $155.8 \pm 0.14$  Ma based on two overlapping fractions on concordia. Slightly discordant older grains may include an inherited older zircon component. Data point error ellipses are  $2\sigma$ . **b)** Photomicrograph of zircons analyzed.

**Table 2.** Results of  $^{40}\text{Ar}/^{39}\text{Ar}$  release during laser step heating of three samples from the SNAP study area.**12MMI2-5-8  
hornblende**

Laser Power(%)	$^{40}\text{Ar}/^{39}\text{Ar}$	1 $\sigma$	$^{37}\text{Ar}/^{39}\text{Ar}$	1 $\sigma$	$^{36}\text{Ar}/^{39}\text{Ar}$	1 $\sigma$	Ca/K	% $^{40}\text{Ar}$ atm	f $^{39}\text{Ar}$	$^{40}\text{Ar}^*/^{39}\text{ArK}$	Age	2 $\sigma$
2.30	486.26	9.28	3.66	0.21	1.457	0.071	6.71	88.49	0.35	56.124	387.95	$\pm 241.57$
2.60	71.76	1.68	1.76	0.09	0.179	0.010	3.23	73.54	0.99	19.008	140.91	$\pm 37.47$
3.00	69.25	0.72	1.60	0.08	0.151	0.006	2.94	64.12	2.38	24.875	182.27	$\pm 23.83$
3.40	31.91	0.23	4.73	0.10	0.020	0.001	8.70	17.18	8.06	26.519	193.70	$\pm 6.01$
3.70	27.42	0.17	5.91	0.10	0.009	0.000	10.88	7.47	45.98	25.481	186.50	$\pm 2.42$
4.00	26.90	0.21	5.50	0.10	0.005	0.000	10.12	4.28	34.59	25.851	189.07	$\pm 2.97$
4.40	28.99	0.27	4.69	0.09	0.011	0.002	8.61	9.72	3.93	26.260	191.90	$\pm 8.68$
5.50	28.71	0.41	4.03	0.11	0.011	0.002	7.40	10.37	3.71	25.807	188.76	$\pm 8.13$
Total/Average	29.453	0.100	3.822	0.036	0.0072	0.0002			100.00	25.715	0.123	

J = 0.0042635  $\pm$  0.0000213 Volume  $^{39}\text{ArK}$  = 0.074 Integrated Date = 188.13  $\pm$  1.71 Ma

Plateau age = 188.2  $\pm$  2.5 Ma (2 $\sigma$ , including J-error of 1%) MSWD = 1.3, probability = 0.25 Includes 98.7% of the  $^{39}\text{Ar}$  steps 3 through 8

Inverse isochron (correlation age) results, plateau steps: Model 1 Solution ( $\pm$  95%-conf.) on 86 points Age = 187.7  $\pm$  3.9 Ma

Initial  $^{40}\text{Ar}/^{36}\text{Ar}$  = 296  $\pm$  30 MSWD = 2.6 Probability = 0.017

**MMI2-8-6  
hornblende**

Laser Power(%)	$^{40}\text{Ar}/^{39}\text{Ar}$	1 $\sigma$	$^{37}\text{Ar}/^{39}\text{Ar}$	1 $\sigma$	$^{36}\text{Ar}/^{39}\text{Ar}$	1 $\sigma$	Ca/K	% $^{40}\text{Ar}$ atm	f $^{39}\text{Ar}$	$^{40}\text{Ar}^*/^{39}\text{ArK}$	Age	2 $\sigma$
2.30	1608.50	49.91	2.51	0.26	4.772	0.210	4.60	87.66	0.26	198.909	1108.30	$\pm 372.06$
2.70	130.10	2.62	1.52	0.14	0.355	0.031	2.79	80.67	0.47	25.177	183.91	$\pm 122.82$
3.10	94.99	1.05	1.04	0.07	0.239	0.018	1.90	74.42	0.80	24.314	177.91	$\pm 75.15$
3.50	81.40	0.82	1.22	0.08	0.186	0.007	2.23	67.60	0.69	26.396	192.36	$\pm 28.34$
3.90	39.92	0.42	3.42	0.08	0.050	0.002	6.27	36.53	3.80	25.397	185.43	$\pm 10.69$
4.20	26.92	0.30	3.71	0.22	0.008	0.000	6.82	7.51	16.60	24.960	182.40	$\pm 4.28$
4.50	25.82	0.17	3.90	0.08	0.005	0.000	7.16	4.15	26.66	24.823	181.44	$\pm 2.54$
4.80	25.79	0.26	3.83	0.07	0.005	0.000	7.03	4.24	22.79	24.765	181.05	$\pm 3.70$
5.10	26.48	0.21	3.47	0.13	0.006	0.000	6.38	5.16	14.82	25.177	183.91	$\pm 3.15$
5.50	28.12	0.20	3.58	0.08	0.012	0.001	6.57	12.06	7.68	24.794	181.25	$\pm 3.90$
6.20	30.88	0.44	3.62	0.09	0.015	0.001	6.64	13.21	5.43	26.871	195.64	$\pm 6.23$
Total/Average	28.708	0.091	2.811	0.028	0.0062	0.0001			100.00	25.021	0.103	

J = 0.0042520  $\pm$  0.0000213 Volume  $^{39}\text{ArK}$  = 0.157 Integrated Date = 182.84  $\pm$  1.44 Ma

Plateau age = 182.1  $\pm$  2.3 Ma (2 $\sigma$ , including J-error of 1%) MSWD = 0.38, probability=0.93 Includes 94.3% of the  $^{39}\text{Ar}$  steps 2 through 10

Inverse isochron (correlation age) results, plateau steps: Model 1 Solution ( $\pm$  95%-conf.) on 9 points Age = 181.4  $\pm$  1.9 Ma

Initial  $^{40}\text{Ar}/^{36}\text{Ar}$  = 302  $\pm$  16 MSWD = 0.35 Probability = 0.007

Table 2. Cont'd.

## MMI12-7-4

## biotite

Laser Power(%)	$^{40}\text{Ar}/^{39}\text{Ar}$	1 $\sigma$	$^{37}\text{Ar}/^{39}\text{Ar}$	1 $\sigma$	$^{36}\text{Ar}/^{39}\text{Ar}$	1 $\sigma$	Ca/K	% $^{40}\text{Ar}$ atm	f $^{39}\text{Ar}$	$^{40}\text{Ar}^*/^{39}\text{ArK}$	Age	2 $\sigma$
2.30	431.97	3.59	0.11	0.03	1.353	0.141	0.21	92.55	0.44	32.179	232.83	± 565.72
2.60	307.24	2.35	0.10	0.03	0.961	0.050	0.18	92.41	0.39	23.318	171.65	± 203.63
2.90	133.23	1.07	0.11	0.03	0.421	0.024	0.20	93.47	0.40	8.705	66.00	± 103.68
3.20	49.96	0.41	0.07	0.02	0.137	0.008	0.12	81.16	0.63	9.413	71.27	± 34.57
3.50	17.13	0.12	0.04	0.01	0.034	0.002	0.07	58.03	1.39	7.190	54.69	± 7.47
3.80	11.04	0.09	0.02	0.00	0.012	0.001	0.03	32.10	3.09	7.497	56.99	± 3.58
4.00	8.91	0.07	0.02	0.00	0.007	0.000	0.04	22.03	3.18	6.944	52.84	± 1.20
4.20	8.17	0.05	0.01	0.00	0.004	0.000	0.03	14.64	3.74	6.972	53.05	± 0.86
4.50	7.83	0.05	0.01	0.00	0.004	0.000	0.01	14.99	7.23	6.657	50.69	± 0.99
4.80	7.44	0.04	0.01	0.00	0.002	0.000	0.01	10.13	11.30	6.686	50.90	± 1.01
5.10	7.33	0.05	0.00	0.00	0.002	0.000	0.01	9.78	10.76	6.612	50.35	± 0.77
5.40	7.45	0.06	0.01	0.00	0.003	0.000	0.02	11.37	9.60	6.604	50.29	± 1.07
5.70	6.85	0.05	0.00	0.00	0.001	0.000	0.01	4.58	13.55	6.533	49.76	± 0.75
6.00	7.04	0.05	0.00	0.00	0.002	0.000	0.00	7.45	8.53	6.513	49.61	± 0.94
6.50	6.96	0.04	0.00	0.00	0.001	0.000	0.01	6.15	12.20	6.532	49.75	± 0.98
7.00	7.44	0.05	0.00	0.00	0.003	0.000	0.01	11.00	5.40	6.618	50.40	± 1.14
7.50	8.06	0.06	0.00	0.00	0.003	0.000	0.00	10.53	3.96	7.207	54.81	± 0.97
8.00	8.00	0.07	0.00	0.00	0.004	0.000	0.00	13.38	4.20	6.929	52.73	± 1.72
Total/Average	7.873	0.014	0.006	0.000	0.0020	0.0000			100.00	6.715	0.019	

$J = 0.0042703 \pm 0.0000214$  Volume  $^{39}\text{ArK} = 0.635$  Integrated Date =  $51.12 \pm 0.28$  Ma

Plateau age =  $50.17 \pm 0.60$  Ma (2 $\sigma$ , including J-error of 1%) MSWD = 1.00, probability = 0.43 Includes 78.6% of the  $^{39}\text{Ar}$  steps 9 through 16 Inverse isochron (correlation age) results, plateau steps: Model 1 Solution ( $\pm 95\%$ -conf.) on 15 points Age =  $49.61 \pm 0.49$  Ma

Initial  $^{40}\text{Ar}/^{36}\text{Ar} = 331 \pm 15$  MSWD = 1.4 Probability = 0.002

long dimension (Fig. 16b). All but the smallest grain provided adequate material for analysis, resulting in the four data points on Figure 16a. Two grains give concordant and overlapping results with a weighted  $^{206}\text{Pb}/^{238}\text{U}$  age of  $155.8 \pm 0.14$  Ma, considered as the best estimate for the age of the rock. The other two grains lie along concordia, give older, non-overlapping results and are interpreted to have older inherited cores or to be older xenocrysts.

Mineralization at Miner Mountain has long been considered a product of the Late Triassic Nicola arc magmatism, but based on the  $^{40}\text{Ar}/^{39}\text{Ar}$  ages above, now may extend into the Early Jurassic ( $\sim 188$  Ma). Nevertheless, a  $\sim 156$  Ma magmatic age for mineralization is much younger than any known or suspected Nicola Group. This anomalously young age may signify: 1) that the sulphide mineralization is remobilized from a deeper, probable Late Triassic source; 2) that the new age is in error, which will be tested by further work on a sample of drill core that intersected the mineralized intrusion; or 3) there exists a  $\sim 156$  magmatic suite with previously unappreciated copper endowment.

Intrusions emplaced around 156 Ma occur in great volumes across southern British Columbia, including the Tulameen, Similkameen and Okanagan complexes. The huge Osprey Lake batholith occupies much of the eastern third of the study area and has returned K-Ar cooling ages from biotite of  $149 \pm 2$  Ma, and from hornblende of  $154 \pm 3$  Ma (Hunt and Roddick, 1988), but a U-Pb crystallization age of  $166 \pm 1$  Ma (Parrish and Monger, 1992).

Sample MMI13-10-8 was collected from a tuffaceous polymictic conglomerate section that sits on, and interfingers with, flow-banded rhyolite (see Spences Bridge Group, section 3.2.1 above). Clasts include limestone, granitoid intrusives, altered mafic volcanic, and those resembling immediately underlying volcanic rock types. Of the twenty-seven grains selected from the zircon separate for analysis, all but two were inspected for evidence of growth zoning and xenocrystic cores (see Mihalynuk et al., 2014b for imagery) before analysis. All LA-ICPMS analyses fall into two  $^{206}\text{Pb}/^{238}\text{U}$  age clusters (Table 4, Fig. 17a) that have age distribution peaks at  $\sim 103$  and  $\sim 220$  Ma. Subsidiary peaks in the older cluster are at  $\sim 190$  and  $\sim$



**Table 4.** Analytical results from zircons of sample MMI13-10-8 by laser ablation (LA) ICP-MS.  $\pm 2\sigma$ , I = integrated error, P = propagated error from all sources.  $^{238}\text{U}/^{206}\text{Pb}$   $\sigma =$  isotopic ratio correlated error

Sample-grain	U ppm $\pm 2\sigma$	Th ppm $\pm 2\sigma$	Pb ppm $\pm 2\sigma$	U/Th $\pm 2\sigma$	$^{207}\text{Pb}/^{235}\text{U}$ $\pm 2\sigma$	$^{206}\text{Pb}/^{238}\text{U}$ $\pm 2\sigma$	$^{206}\text{Pb}/^{238}\text{U}$ $\pm 2\sigma$ I	$^{206}\text{Pb}/^{238}\text{U}$ $\pm 2\sigma$ P	$^{206}\text{Pb}/^{238}\text{U}$ $\sigma$	$^{206}\text{Pb}/^{238}\text{U}$ Ma	$\pm 2\sigma$	$\pm 2\sigma$ P	$^{207}\text{Pb}/^{206}\text{Pb}$ $\pm 2\sigma$	$\pm 2\sigma$ I	$\pm 2\sigma$ P	$^{207}\text{Pb}/^{235}\text{U}$ Ma									
MMI13-10-8-1	189	4.8	53	1.4	25.2	2	3.196	0.069	0.2300	0.0170	0.020	0.035	0.0010	0.0014	0.02225	223.2	6.4	8.9	0.0496	0.0040	0.0047	0.43117	206	14	17
MMI13-10-8-2	300.1	9	71.7	3.4	35.5	2.6	3.76	0.12	0.2620	0.0140	0.019	0.035	0.0010	0.0014	0.12221	219.8	6.0	8.5	0.0547	0.0033	0.0043	0.48831	233	11	15
MMI13-10-8-3	203.8	5.7	48.7	1.7	20.1	1.8	3.656	0.098	0.2070	0.0160	0.019	0.030	0.0010	0.0013	0.14620	193.1	5.9	7.8	0.0506	0.0042	0.0049	0.37341	184	14	16
MMI13-10-8-4	262.9	8.7	38.5	2.2	10.9	1.9	5.85	0.26	0.0960	0.0130	0.010	0.017	0.0008	0.0008	0.05267	108.3	5.2	5.0	0.0453	0.0066	0.0039	0.46334	93	12	8.8
MMI13-10-8-5	467	13	153.8	3.8	77.8	4.1	2.637	0.049	0.2430	0.0110	0.016	0.034	0.0008	0.0013	0.14006	215.4	5.0	7.9	0.0512	0.0025	0.0037	0.35645	218.4	9.4	14
MMI13-10-8-6	835	21	479	20	272	12	1.58	0.049	0.2599	0.0095	0.016	0.036	0.0008	0.0013	0.28987	228.1	4.7	7.8	0.0509	0.0018	0.0032	0.29251	232.6	7.6	13
MMI13-10-8-7	4650	120	6270	160	3099	91	0.6209	0.0092	0.2298	0.0046	0.012	0.032	0.0005	0.0011	0.57544	205.9	3.4	6.6	0.0505	0.0009	0.0028	0.3304	209.5	3.8	10
MMI13-10-8-8	269.2	8.9	50.9	3.3	15.4	1.8	4.97	0.27	0.1320	0.0120	0.012	0.017	0.0007	0.0007	0.15794	109.5	4.2	4.7	0.0583	0.0055	0.0056	0.42447	125	11	11
MMI13-10-8-9	159.2	4.3	67.5	2.4	12	1.4	2.07	0.049	0.1130	0.0130	0.014	0.016	0.0008	0.0009	0.08085	103.9	5.1	5.6	0.0670	0.0100	0.011	1	105	11	12
MMI13-10-8-10	401	15	154.7	6.7	58.7	4.1	2.285	0.054	0.2670	0.0120	0.018	0.035	0.0009	0.0013	0.09691	218.9	5.6	8.2	0.0561	0.0029	0.0041	0.43364	237.6	9.9	14
MMI13-10-8-11	544	23	690	44	188	13	0.86	0.031	0.2220	0.0110	0.015	0.032	0.0008	0.0012	0.25919	200.5	5.0	7.3	0.0500	0.0024	0.0034	0.23948	203.7	8.9	12
MMI13-10-8-12	283.3	9.6	146.9	5.7	45.5	3.1	1.977	0.038	0.2490	0.0170	0.021	0.035	0.0009	0.0013	0.16182	219.8	5.6	8.1	0.0508	0.0036	0.0045	0.311	220	14	17
MMI13-10-8-13	916	46	675	42	94.1	6.9	1.487	0.035	0.1063	0.0055	0.008	0.016	0.0004	0.0006	0.18375	100.8	2.7	3.9	0.0498	0.0028	0.0038	0.34982	102.4	5.1	7.2
MMI13-10-8-14	302.8	8.6	1527	58	488	22	2.215	0.0043	0.2950	0.0160	0.022	0.035	0.0009	0.0013	0.10397	223.3	5.8	8.4	0.0613	0.0037	0.0047	0.30504	259	13	17
MMI13-10-8-15	349	31	339	37	90	10	2.28	0.22	0.2500	0.0180	0.022	0.034	0.0011	0.0014	0.05648	214.7	6.7	8.9	0.0544	0.0043	0.0051	0.47547	219	15	18
MMI13-10-8-16	453.9	9.7	234.4	8.3	38.5	3	2.181	0.068	0.1175	0.0080	0.010	0.016	0.0005	0.0007	0.02016	103.2	3.2	4.3	0.0535	0.0039	0.0047	0.34333	111	7.2	8.8
MMI13-10-8-17	145	4.4	98.5	3	30.4	2.6	1.615	0.043	0.2470	0.0240	0.024	0.037	0.0017	0.0017	0.14168	234.0	10.0	10.0	0.0509	0.0051	0.0051	0.41179	217	19	19
MMI13-10-8-18	294.8	6.1	147.2	3	45.8	2.8	2.087	0.04	0.2620	0.0150	0.020	0.035	0.0009	0.0013	0.14539	221.8	5.7	8.3	0.0551	0.0034	0.0044	0.42291	236	12	16
MMI13-10-8-19	644	20	457	21	121	7.6	1.499	0.037	0.2161	0.0094	0.014	0.030	0.0006	0.0011	0.08504	188.7	4.0	6.6	0.0521	0.0024	0.0036	0.37345	198.1	7.9	12
MMI13-10-8-20	397	14	207.1	9	75.8	5.2	1.863	0.047	0.2470	0.0150	0.019	0.035	0.0009	0.0013	0.13043	220.6	5.8	8.2	0.0509	0.0031	0.004	0.29094	224	12	15
MMI13-10-8-21	161	10	101.2	7.9	32.7	4.7	1.587	0.07	0.2300	0.0300	0.120	0.036	0.0023	0.0025	0.23972	229.0	14.0	15.0	0.0473	0.0064	0.018	0.1361	203	25	56
MMI13-10-8-22	181.7	9.3	109.7	7.9	19.8	3	1.608	0.076	0.1000	0.0190	0.017	0.018	0.0012	0.0012	0.06835	117.0	7.6	7.3	0.0450	0.0088	0.012	0.49225	97	18	15
MMI13-10-8-23	1521	59	938	44	151.5	9.9	1.513	0.031	0.1067	0.0053	0.007	0.016	0.0004	0.0006	0.24527	103.7	2.7	3.9	0.0467	0.0024	0.0034	0.31919	102.7	4.9	6.7
MMI13-10-8-24	710	130	570	100	137	26	1.899	0.06	0.2710	0.0230	0.025	0.036	0.0012	0.0015	0.15448	225.9	7.4	9.3	0.0559	0.0048	0.0052	0.22966	236	18	20
MMI13-10-8-25	388	48	124	5.1	32.4	2.9	3.74	0.31	0.2300	0.0160	0.019	0.036	0.0010	0.0014	0.04161	228.6	6.4	9.0	0.0490	0.0037	0.0044	0.40856	209	13	16
MMI13-10-8-26	456	36	275	28	31.8	4.3	2.34	0.1	0.1200	0.0120	0.013	0.016	0.0008	0.0009	0.15848	104.0	5.0	5.6	0.0567	0.0058	0.0066	0.55626	114	11	12
MMI13-10-8-27	373.4	9	200.3	7.2	23.5	2.9	2.337	0.074	0.1270	0.0130	0.014	0.017	0.0006	0.0008	0.03596	107.7	4.1	5.0	0.0600	0.0064	0.0068	0.40293	119	11	12

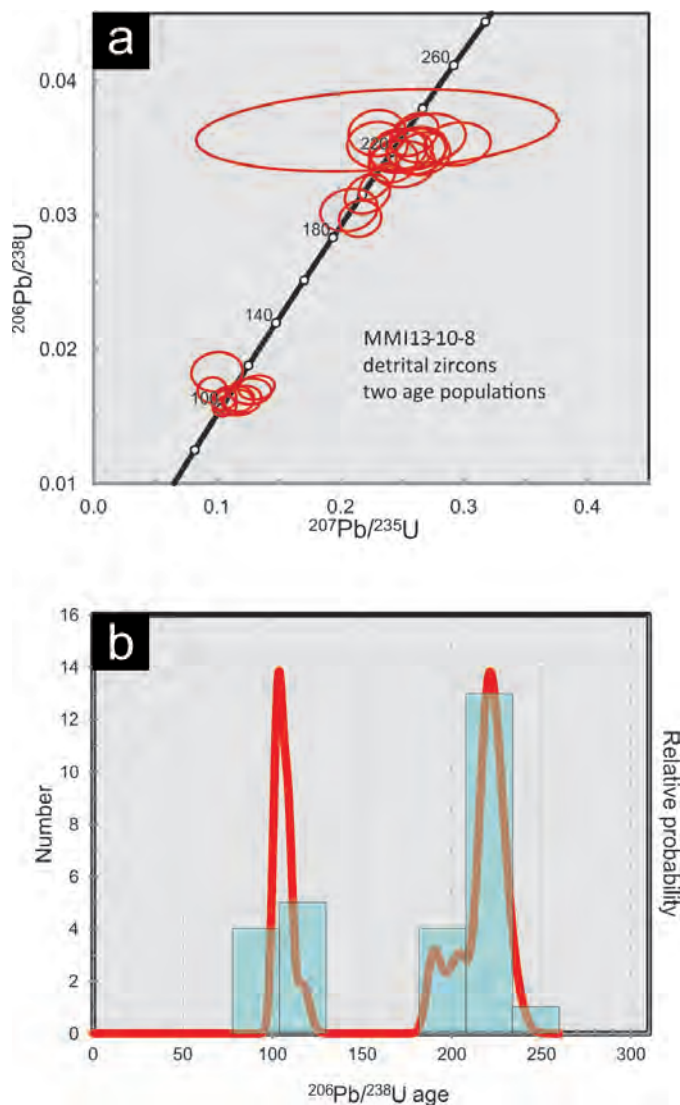


**Fig. 17.** Laser Ablation (LA-ICPMS) U-Pb isotopic determination of ages of detrital zircons separated from a sample of conglomerate, MMI13-10-8. **a)** Isochron plot of individual zircons analyzed with clustering of data into two populations. Data point error ellipses are  $2\sigma$ . **b)** Age distribution and “relative probability” plot showing two main populations, 103 and ~220 Ma, but also a ~190 Ma population, supporting the Early Jurassic cooling ages (see Fig. 14) and extension of the Nicola arc volcanism into the Jurassic. Provenance for the 103 Ma zircons is the Spences Bridge Group (103 Ma, Diakow and Barrios, 2008) which interfingers with, and overlies the Nicola Group formerly considered to be of Late Triassic age (229-201Ma, timescale of Cohen et al., 2013).

205 Ma.

All age distribution peaks can be easily linked to probable sources. A lack of grains younger than 103Ma and a dense cluster at 103 Ma, which is the age of the Spences Bridge Group (Diakow and Barrios, 2008), confirm our geological observations that point to synvolcanic (tuffaceous) sedimentation coeval with Spences Bridge Group felsic volcanism. All older grains were likely derived from the underlying Allison Lake pluton or nearby Nicola Group volcanic arc rocks. From a similar polymictic conglomerate

near Dry Lake, Preto (1979) sampled a clast lithologically identical to the Allison Lake pluton. This clast yielded a K/Ar (muscovite) age of  $207 \pm 10$  Ma (recalculated from  $203 \pm 5$  Ma, using new decay constants and error estimates, Breitsprecher and Mortensen, 2004), confirming derivation from the plutonic roots of the underlying arc. Importantly, the ~190 Ma sub-peak supports our interpretation of 188 Ma cooling age of sample MMI12-5-8 (see Hornblende and biotite  $^{40}\text{Ar}/^{39}\text{Ar}$ , above) as a crystallization age, and indicates exposure of this or a coeval magmatic unit to erosional levels during Spences Bridge deposition.

## 8. Mineralization

In 2013, the most intensive mineral exploration project conducted in the study area was by Seago Resources Inc. at their Miner Mountain deposit. The most significant assayed interval from percussion drilling of 34 holes was: 30m of 0.31% Cu and 0.15 g/t Au from 32 m to the end of hole at 62m in PDH-13-109 (Stevenson, 2013). For an overview of the geology and mineralization at Miner Mountain see Mihalynuk and Logan (2013a) and the Seago Resources Inc. website: <http://www.seagoresources.com/>. Here we present new observations from known and previously unreported mineral occurrences. Results from mineralized samples submitted for analysis by ICP-MS are presented in Table 1 and a complete array of elements analyzed, plus determinations by Instrumental Neutron Activation Analysis are reported in Mihalynuk et al. (2014a).

### 8.1. Rats prospect (MINFILE 092HNE176)

The Rats porphyry Cu-Au prospect is 12 km northeast of Princeton in a panel of Nicola volcanic and intrusive rocks that are intruded on the east by Early Cretaceous granodiorite of the Summers Creek pluton. Within one kilometre to the west, they are in fault contact with Eocene volcanic and sedimentary rocks of the Princeton Group (Fig. 3). Cu-Au-Ag ± Mo mineralization is hosted in northwest-trending brittle shear zones, sheeted veins, and breccia zones in massive plagioclase > pyroxene phyric basalt and mafic fragmental rocks that are hornfelsed within ~100 m of the fine-grained monzodiorite border phase of the Summers Creek pluton. A post-mineral feldspar-hornblende-quartz porphyry dike intrudes the mineralized zone.

Two styles of alteration and mineralization are recognized at the Rats, one with the assemblage K-feldspar, magnetite, actinolite and epidote with chalcocopyrite (JLO13-26-6, 26-80), the other with albite bleaching, epidote, magnetite, pyrite, and chalcocopyrite in quartz and calcite veins/stockworks (JLO13-26-6-2, 26-9 and 26-11). Higher gold and silver values appear to be linked to higher copper values. Analyses of Rats mineralization reveals some of the highest Mo values obtained in the study area (Table 1).

### 8.2. Hit prospect (MINFILE 092HNE053)

Southeast of Mystery Lake, overburden has been scraped from a north-northwest-elongate area, ~400 m by 75 m, down to bedrock (Fig. 18a). Exposed are a series of en echelon quartz veins (Fig. 18 inset) in scaly calcareous phyllite containing abundant irregular quartz veinlets and possibly sparse quartz eyes. Trenches further expose white and rusty quartz veins. Individual quartz veins are up to ~1.25 m thick (thicker

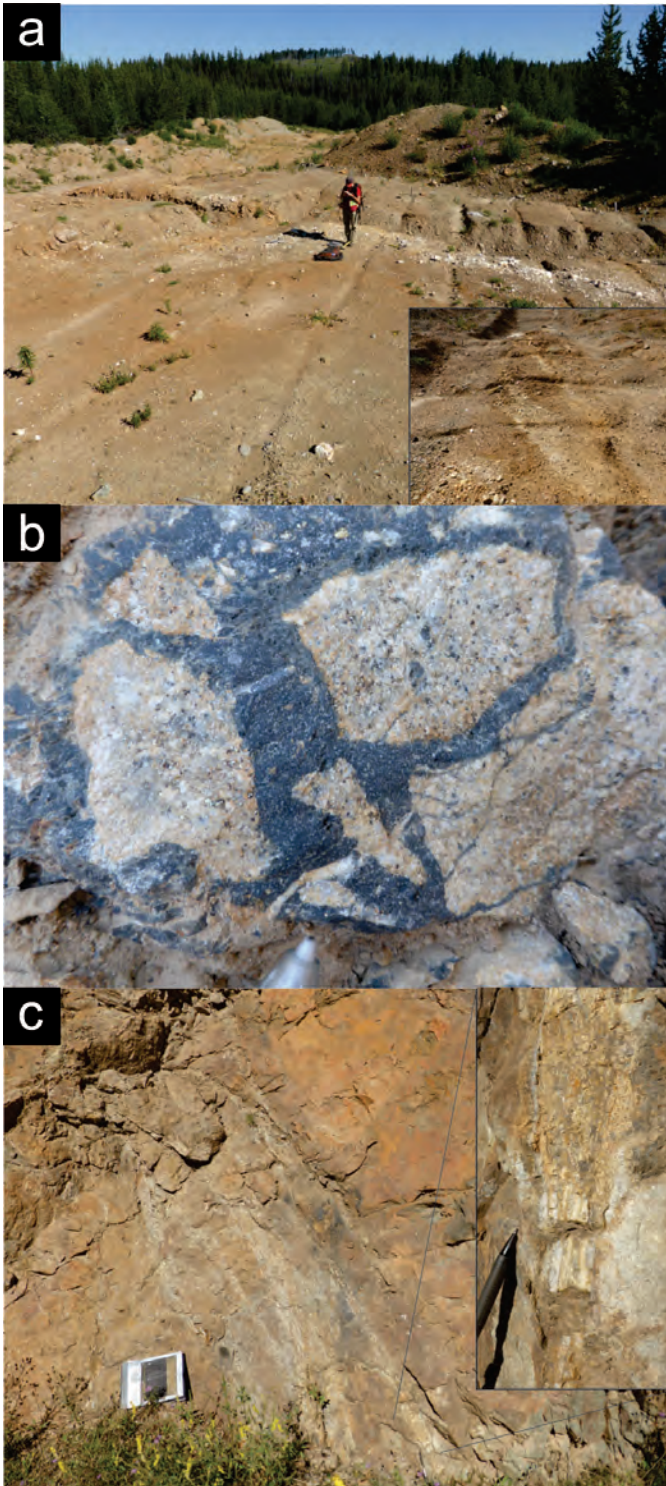


**Fig 18. a)** View to the north of the cleared area and exposed white precious and base metal-bearing quartz vein material at the Hit prospect. Inset is a view to the south showing the en-echelon nature of intermediate-sized veins. **b)** Tourmaline-cemented breccia at the Rum porphyry copper occurrence. **c)** Set of sheeted quartz-carbonate precious metal epithermal veins in the basal Spences Bridge Group. Inset shows vein detail.

where they intersect) and contain patchy base metal sulphides (visually estimated in most places as < 2%), mainly as galena,

pyrite, sphalerite and chalcopyrite. A sample collected from one of the large mineralized veins returned 1.8 ppm Au, 21.6 ppm Ag, 0.5 % Pb, and 0.3% Zn (MMI13-19-1, Table 1).

### 8.3. Rum prospect (MINFILE 092HNE099)

The Rum prospect is ~ five km south of Misesezula Lake and one kilometre west of Summers Creek fault. It comprises a broad zone of tourmaline-pyrite alteration extending from quartz diorite with spotty but ubiquitous copper staining at least 400 m into Nicola Group country rocks. Contrasting alteration in the country rocks is epidote-chlorite-actinolite=prehnite, a mineral assemblage typical of the low-grade regional metamorphism in the Late Triassic section. Within the white and rusty orange-weathering intrusion, tourmaline forms rosettes, aphanitic matrix flood, or cement between secondary breccia fragments (Fig. 18b).

Medium-grained holocrystalline plagioclase and chloritized mafic minerals comprise most of the rocks, with granular magnetite 5-10% (variably oxidized to hematite) and intercrystalline quartz (~ 5-10%). Plagioclase is replaced by calcite and white mica. Zones of chalcopyrite and rare bornite are disseminated or less commonly in veins up to a centimetre thick visible in outcrop and freshly broken surfaces. K-feldspar flooding is locally intense and magnetite breccia is developed in metre-wide zones. Samples collected from adjacent altered country rocks and mineralized portions of the altered intrusion contain up to 0.85% Cu, 12.5 ppm Ag, and 0.39 ppm Au (MMI13-19-11, 19-12, 20-1, 20-2, 20-3, 21-1, 21-2, 21-3, 21-4 in Table 1) with highest values coming from the intrusions.

### 8.4. Exhalative mineralization

In the Nicola Group near Coalmont, bimodal, submarine volcanism, and possible exhalite (Fig. 5b) containing minor iron and copper sulphides are indicators of an environment in which volcanogenic massive sulphides (VMS) could accumulate (for lithologic descriptions see “Felsic tuffite” above). Toward the east, an extensive area underlain by rhyolite (Fig. 3) is pyritic, and weathers to locally broad gossans. About a kilometre southeast of Coalmont this rhyolite belt passes along strike into a section of mafic tuffite containing thin layers of magnetite and disseminated chalcopyrite that could be exhalative. Samples collected from this unit range from 1 to 14.5 % Fe and contain up to 0.33% Cu and 0.56 ppm Ag (MMI13-37-9a, 9b, MMI13-38-8b, 10, Table 1). Whether or not the magnetite-chalcopyrite layers are of exhalative origin has not been conclusively determined. They could be related to the sub-surface extent of the Boulder intrusion, the surface expression of which terminates in this same area. Because this weakly mineralized prospect lacks elevated Ba, Se, and Co (see Mihalynuk et al., 2014a), which are common VMS pathfinder elements, an intrusive association for the magnetite-chalcopyrite layers should be considered. However, evidence of a bimodal submarine environment with possible cherty exhalite supports a VMS-related origin. Further investigation is anticipated in 2014, including sampling of the rhyolite for age determination. Detrital zircon geochronology of the quartz-bearing clastic unit interbedded with cherty “exhalite” is in progress.

### 8.5. Cretaceous (?) epithermal veins

Potential for epithermal precious metal mineralization has been demonstrated elsewhere in the Spences Bridge Group (Diakow and Barrios, 2009) and mapping as part of this project has revealed similar quartz vein systems.

Near the junction of Highway 5A and Pike Mountain Forest Service Road (at Summit Lake, Fig. 3), a set of sheeted, 0.1 – 15cm thick, banded quartz and quartz-carbonate veins (Fig. 18c and inset) cuts pyritic, coarse basal breccia of the Spences Bridge Group adjacent to a faulted unconformity with the Allison Lake pluton. Rounded to angular boulders and blocks of pink Allison Lake intrusion are admixed with aphanitic green volcanic blocks and sparse pyrite clasts (< 5 cm in long dimension) that have a foliated fabric, possibly originating as entrained fragments of foliated basement that was replaced by pyrite. Orange-weathering, green matrix is probably predominantly ash. Weak carbonate alteration and a crisscrossing network of carbonate veinlets affect the local outcrops. A ~ one metre chip sample collected across the most intensely veined part of the outcrop (center of Fig. 18c) returned 6.3 ppm Ag and 0.1 ppm Au with elevated Te (3.8 ppm), As (246 ppm), and Hg (80 ppb, MMI13-32-1, Table 1).

Impressive epithermal textures, albeit without significant precious metal content, are displayed by the vein system at LDI13-8.3 (UTM 673718E, 549398N, Fig. 3) at an isolated knoll of aphanitic andesite, considered to be part of the lower Spences Bridge volcanic unit. Andesite crosscut by spaced quartz veinlets resembles a black, fine-grained clastic rock. The quartz is translucent with various forms including: dismembered veinlets with ductile deformation fabrics alternating with narrow black ribbons of silicified country rock (Fig. 19a); narrow gash veinlets in fractured black silicified country rock; and angular fragments with diffuse outlines in quartz breccia (Fig. 19b). Silica replacing former bladed calcite (Fig. 19c) occupies vugs in all quartz varieties. Sericite (?) -altered fragments in the dismembered example, and host rock domains attendant to quartz apparently have undergone moderate silicification.

### 9. Conclusions

Principal observations arising from the orientation survey in 2012 and mapping in 2013, lead to the following conclusions.

1). Nicola arc volcanism is not restricted to the Late Triassic, but extends into the Lower Jurassic with the addition of hornblende phenocrysts in mafic extrusive rocks.

2). Felsic volcanism, previously thought to be characteristic of the western Nicola belt, apparently extends into the eastern belt. However, we have yet to verify the age of the eastern rhyolite.

3). Near the community of Coalmont, evidence for exhalative mineralization warrants further evaluation for VMS settings in probable Late Triassic bimodal volcanogenic strata.

4). Mineralized intrusive systems, such as at Dillard Creek, are Early Jurassic, significantly expanding the age range of arc rocks prospective for porphyry copper mineralization.

5). Discovery of epithermal-style quartz veins hosted by mid-Cretaceous Spences Bridge strata emphasizes the regional significance of this sequence for precious metal vein exploration.

6). In addition to block faulting, ductile deformation,

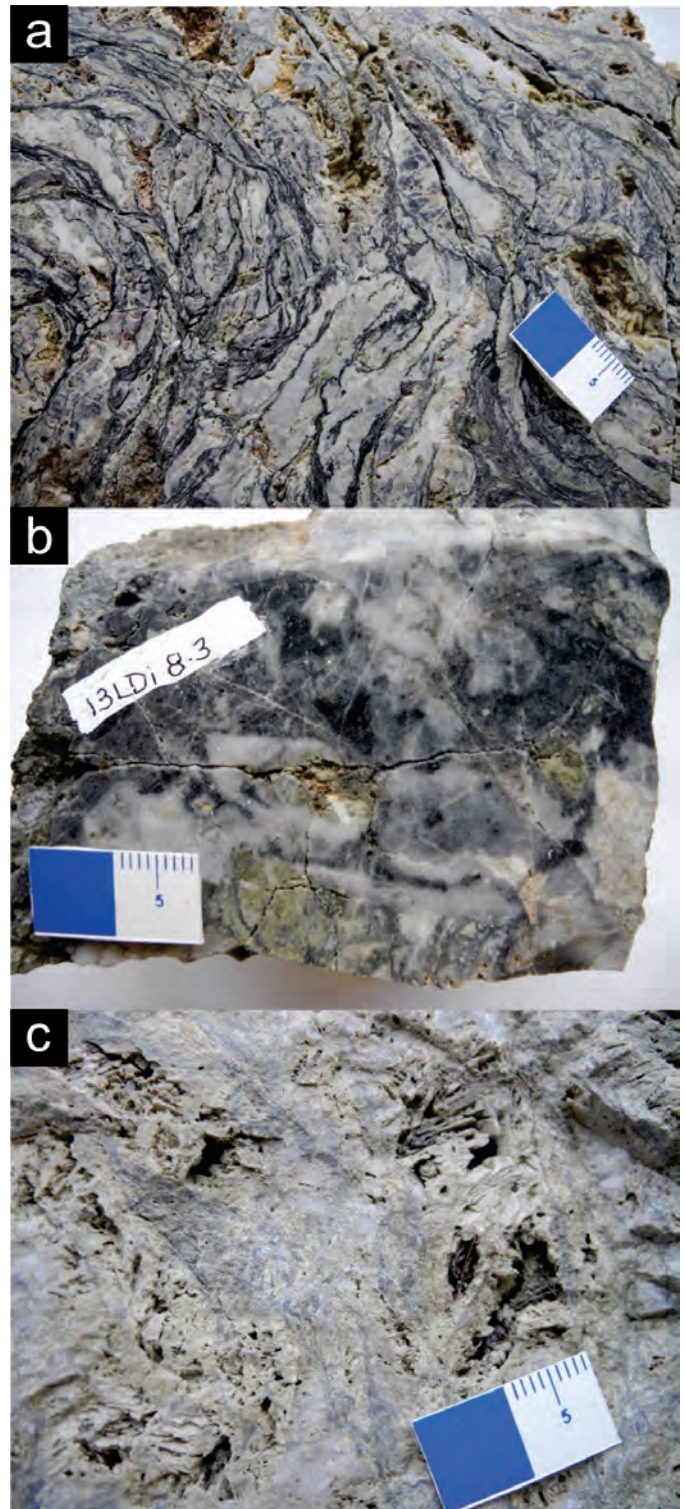


**Fig. 19.** Epithermal-style vein quartz, hosted by early Cretaceous volcanic rocks of the Spences Bridge Group, 15 km northeast of Princeton (UTM location 673718E, 5493984N). **a)** Dismembered and folded vein quartz containing vugs infilled with bladed quartz after calcite. **b)** Diffuse quartz fragments comprising breccia in a siliceous black, fine clastic matrix. **c)** Close-up of vuggy texture with bladed calcite crystals now replaced by silica.

including thrust faulting and folding, was important in redistributing Nicola arc facies.

7). Extensional deformation of Eocene age (and perhaps as young as Miocene) affects the entire width of the arc so far investigated. Unravelling this deformation will be an important step in reconstructing the Late Triassic mineralizing landscape of the Nicola arc.

### Acknowledgments

We are indebted to past workers in the southern Nicola arc, especially J. Monger and V. Preto, both of whom have generously shared their time and knowledge with us in the field. Our corporate partners Segor Resources Inc. are generous supporters of the Southern Nicola Arc Project.

### References cited

- Bordet, E.-J., Mihalynuk, M.G., Hart, C.J.R., Mortensen, J.K., Friedman, R.M., and Gabites, J., 2013. Chronostratigraphy of Eocene volcanism, Central British Columbia. *Canadian Journal of Earth Sciences*, in press. doi: 10.1139/cjes-2013-0073.
- Breitsprecher, K., and Mortensen, J.K., 2004. BCAGE 2004A-1-a database of isotopic age determinations for rock units from British Columbia. British Columbia Ministry of Energy and Mines, British Columbia Geological Survey, Open File, v. 3.
- Brown, R., and Journeay, J., 1987. Tectonic Denudation of the Shuswap Metamorphic Terrane of Southeastern British-Columbia. *Geology*, 15, 142–146. doi: 10.1130/0091-7613(1987)15<142:TD OTSM>2.0.CO;2.
- Cho, M., and Liou, J., 1987. Prehnite Pumpellyite to Greenschist Facies Transition in the Karmutsen Metabasites, Vancouver Island, BC. *Journal of Petrology*, 28, 417–443.
- Church, B.N., 1973. Geology of the White Lake Basin. British Columbia Department of Mines and Petroleum Resources, Bulletin 61, 120 p.
- Cohen, K.M., Finney, S.C., Gibbard, P.L., and Fan, J.X., 2013. The ICS International Chronostratigraphic Chart. *Episodes*, 36, 199–204.
- Crowley, J.L., Schoene, B. and Bowering, S.A., 2007. U-Pb dating of zircon in the Bishop Tuff at the millennial scale. *Geology*, 35, 1123–1126.
- Davis, G.A., Monger, J.W.H., and Burchfiel, B.C. 1978. Mesozoic construction of the Cordilleran “collage,” central British Columbia to central California. In: *Mesozoic paleogeography of the western United States*. Edited by D.G. Howell and K.A. McDougall. Society of Economic Paleontologists and Mineralogists, Pacific Coast Paleogeography Symposium, 2, 1–32.
- Diakow, L.J. and Barrios, A., 2008. Geology, Spences Bridge Group southwest of Merritt, British Columbia (parts of NTS 092H/14, 15 and 092I/2,3). BC Ministry of Energy Mines and Petroleum Resources, British Columbia Geological Survey, Open File 2008-8, 1:50 000 scale.
- Diakow, L.J. and Barrios, A. 2009. Geology and Mineral Occurrences of the Mid-Cretaceous Spences Bridge Group near Merritt, Southern British Columbia (Parts of NTS 092H/14, 15; 092I/2, 3). In: *Geological Fieldwork 2008*, BC Ministry of Energy Mines and Petroleum Resources, British Columbia Geological Survey, Paper 2009-1, pp. 63–79.
- Enkin, R.J., 2006. Paleomagnetism and the case for Baja British Columbia: Paleogeography of the North American Cordillera: Evidence For and Against Large-Scale Displacements. In: *Geological Association of Canada, Special Paper*, 46, 233–253.
- Ferri, F., 1997. Nina Creek Group and Lay Range Assemblage, north-central British Columbia: remnants of late Paleozoic oceanic and arc terranes: *Canadian Journal of Earth Sciences*, 34, 854–874. doi: 10.1139/e17-070.
- Gerstenberger, H., and Haase, G., 1997. A Highly effective emitter substance for mass spectrometric Pb isotopic ratio determinations. *Chemical Geology*, 136, 309–312.
- Greig, C.J., Armstrong, R.L., Harakal, J.E., Runkle, D., and der Heyden, P. van, 1992. Geochronometry of the Eagle Plutonic Complex and the Coquihalla area, southwestern British Columbia. *Canadian Journal of Earth Sciences*, 29, 812–829.
- Halliday, A.N., Davidson, J.P., Hildreth, W., and Holden, P., 1991. Modelling the petrogenesis of high Rb/Sr silicic magmas. *Chemical Geology*, 92, 107–114. doi: 10.1016/0009-2541(91)90051-R.
- Hills, L.V., 1965. Source of the Allenby Formation, Princeton Coalfield, British Columbia. *Bulletin of Canadian Petroleum Geology*, 13, 271–279.
- Hunt, P.A., and Roddick, J.C., 1988. A compilation of K–Ar ages: Radiogenic age and isotopic studies. *Geological Survey of Canada, Report*, 18, 127–153.
- Ickert, R.B., Thorkelson, D.J., Marshall, D.D., and Ullrich, T.D., 2009. Eocene adakitic volcanism in southern British Columbia. Remelting of arc basalt above a slab window. *Tectonophysics*, 464, 164–185.
- Jaffey, A.H., Flynn, K.F., Glendenin, L.E., Bentley, W.C., and Essling, A.M., 1971. Precision measurement of half-lives and specific activities of <sup>235</sup>U and <sup>238</sup>U. *Physical Review*, C4, 1889–1906.
- Koppers, Anthony A.P., 2002. ArArCALC – software for <sup>40</sup>Ar/<sup>39</sup>Ar age calculations. *Computers and Geosciences*, 28, 605–619.
- Kuiper, K.F., Deino, A., Hilgen, F.J., Krijgsman, W., Renne, P.R., Wijbrans, J.R., 2008. Synchronizing rock clocks of earth history. *Science*, 320, 500–504.
- Le Bas, M.J., 2000. IUGS Reclassification of the High-Mg and Picroitic Volcanic Rocks. *Journal of Petrology*, 41, 1467–1470. doi: 10.1093/petrology/41.10.1467.
- Ludwig, K., 2003. Isoplot/Ex, version 3: A geochronological toolkit for Microsoft Excel. University of California at Berkeley, Geochronology Center, Special Publication No. 4, kludwig@bgc.org.
- Massey, N.W.D., MacIntyre, D.G., Desjardins, P.J., and Cooney, R.T., 2005. Digital geology map of British Columbia: Whole province. British Columbia Ministry of Energy, Mines and Petroleum Resources, Geofile 2005-1.
- Massey, N.W.D., and Oliver, S.L., 2010. Southern Nicola Project: Granite Creek Area, southern British Columbia (Parts of NTS 092H/07, 10). In: *Geological Fieldwork 2009*, BC Ministry of Energy and Mines, British Columbia Geological Survey, Paper 2010-1, pp. 113–126.
- Mathews, W.H., 1989. Neogene Chilcotin basalts in south-central British Columbia: geology, ages, and geomorphic history: *Canadian Journal of Earth Sciences*, 26, 969–982. doi: 10.1139/e89-078.
- Mattinson, J.M., 2005. Zircon U-Pb chemical abrasion (“CA-TIMS”) method: Combined annealing and multi-step partial dissolution analysis for improved precision and accuracy of zircon ages. *Chemical Geology*, 220, 47–66.
- McMechan, R.D., 1983. Geology of the Princeton Basin. BC Ministry of Energy, Mines, and Petroleum Resources, British Columbia Geological Survey, Paper 1983-3, 52 p.
- Mihalynuk, M.G., Nelson, J., and Diakow, L.J., 1994. Cache Creek Terrane entrapment: Oroclinal paradox within the Canadian Cordillera. *Tectonics*, 13, 575–595.
- Mihalynuk, M.G., Mountjoy, K.J., Smith, M.T., Currie, L.D., Gabites, J.E., Tipper, H.W., Orchard, M.J., Poulton, T.P., and Cordey, F., 1999. Geology and mineral resources of the Tagish Lake area (NTS 104M/ 8,9,10E, 15 and 104N/ 12W), northwestern British Columbia. B C Ministry of Energy and Mines, 217 p.
- Mihalynuk, M., Erdmer, P., Ghent, E.D., Cordey, F., Archibald, D.A., Friedman, R.M., and Johannson, G.G., 2004. Coherent French Range blueschist: Subduction to exhumation in < 2.5 m.y.?. *Geological Society of America Bulletin*, 116, 910–922.
- Mihalynuk, M.G., Friedman, R.M., Gabites, J.E., and Logan, J.M., 2014b. Southern Nicola Arc Project 2013: Geochronological data. BC Ministry of Energy and Mines, British Columbia Geological Survey, Geofile 2014-3.

- Mihalynuk, M.G., and Ghent, E.D., 1996. Regional depth-controlled hydrothermal metamorphism in the Zymoetz River area, British Columbia. *Canadian Journal of Earth Sciences*, 33, 1169-1184.
- Mihalynuk, M.G., and Logan, J.M., 2013a. Geological setting of Late Triassic Cu-Au porphyry mineralization at Miner Mountain, Princeton. In: *Geological Fieldwork 2012*, BC Ministry of Energy, Mines and Natural Gas, British Columbia Geological Survey, Paper 2013-1, pp. 81-96.
- Mihalynuk, M.G., and Logan, J.M., 2013b. Geological setting of Late Triassic Cu-Au porphyry mineralization at the Dillard-Primer prospects near Merritt. In: *Geological Fieldwork 2012*, BC Ministry of Energy, Mines and Natural Gas, British Columbia Geological Survey, Paper 2013-1, pp. 97-114.
- Mihalynuk, M.G., and Logan, J.M., 2013c. Litho-geochemical data from porphyry environments between Princeton and Merritt: BC Ministry of Energy, Mines and Natural Gas, British Columbia Geological Survey, Geofile 2013-05.
- Mihalynuk, M.G., Logan, J.M., and Diakow, L.D., 2014a. Southern Nicola Arc Project 2013: Geochemical data. BC Ministry of Energy and Mines, British Columbia Geological Survey, Geofile 2014-2.
- Monger, J.W.H., and Ross, C.A., 1971. Distribution of fusulinaceans in the western Canadian Cordillera. *Canadian Journal of Earth Sciences*, 8, 259-278.
- Monger, J.W.H., Souther, J.G., and Gabrielse, H., 1972. Evolution of the Canadian Cordillera: a plate-tectonic model. *American Journal of Science*, 272, 577-602.
- Monger, J.W.H., 1977. Upper Paleozoic rocks of the western Canadian Cordillera and their bearing on Cordilleran evolution. *Canadian Journal of Earth Sciences* 14, 1832-1859.
- Monger, J.W.H., 1989. Geology, Hope, British Columbia. Geological Survey of Canada, Map 41-1989, sheet 1, scale 1:250 000.
- Moss, P.T., Greenwood, D.R., and Archibald, S.B., 2005. Regional and local vegetation community dynamics of the Eocene Okanagan Highlands (British Columbia – Washington State) from palynology. *Canadian Journal of Earth Sciences*, 42, 187-204. doi: 10.1139/e04-095.
- Mundil, R., Ludwig, K. R., Metcalfe, I., and Renne, P. R., 2004. Age and timing of the Permian Mass Extinctions: U/Pb Dating of Closed-System Zircons. *Science*, 305, 1760-1763.
- Nixon, G.T., Archibald, D.A., and Heaman, L.M., 1993. <sup>40</sup>Ar-<sup>39</sup>Ar and U-Pb geochronometry of the Polaris alaskan-type complex, British Columbia; precise timing of Quesnellia-North America interaction. Geological Association of Canada, Mineralogical Association of Canada; Program with Abstracts 76.
- Parrish, R.R., and Monger, J.W.H., 1992. New U-Pb dates from southwestern British Columbia: Radiogenic age and isotopic studies. Report 5, 87-108.
- Patton, C., Hellstrom, J., Paul, B., Woodhead, J. Hergt, J., 2011. Iolite: freeware for the visualization and processing of mass spectrometry data. *Journal of Analytical Atomic Spectroscopy*, 26, 2508-2518.
- Pearce, J.A., Harris, N.B.W., Tindle, A.G., 1984. Trace element discrimination diagrams for the tectonic interpretation of granitic rocks. *J. Petrol.* 25, 956-983.
- Preto, V.A., 1979. Geology of the Nicola Group between Merritt and Princeton: BC Ministry of Energy, Mines and Petroleum Resources, British Columbia Geological Survey, Bulletin 69, 90 p.
- Ray, G.E., and Dawson, G.L., 1994. The geology and mineral deposits of the Hedley gold skarn district, southern British Columbia: British Columbia Ministry of Energy, Mines and Petroleum Resources, British Columbia Geological Survey, Bulletin 87, 156 p.
- Read, P.B., and Okulitch, A.V., 1977. The Triassic unconformity of South-central British Columbia. *Canadian Journal of Earth Sciences*, 14, 606-638.
- Rice, H.M.A., 1960. Geology and mineral deposits of the Princeton map area, British Columbia. Geological Survey of Canada, Memoir 243, 136 p.
- Ricketts, B.D., Evenchick, C.A., Anderson, R.G., and Murphy, D.C., 1992. Bowser Basin, northern British Columbia; constraints on the timing of initial subsidence and Stikinia-North America Terrane interactions. *Geology*, 20, 1119-1122.
- Russell, L.S., 1935. A middle Eocene mammal from British Columbia. *American Journal of Science*, 29, 54-55.
- Schiarizza, P., Bell, K., and Bayliss, S., 2009. Geology and mineral occurrences of the Murphy Lake area, south-central British Columbia (NTS 093A/03). In: *Geological Fieldwork 2008*, British Columbia Ministry of Energy, Mines and Petroleum Resources, British Columbia Geological Survey, Paper 2009-1, pp.169-188.
- Scoates, J.S., and Friedman, R. M., 2008. Precise age of the platiniferous Merensky Reef, Bushveld Complex, South Africa, by the U-Pb ID-TIMS chemical abrasion ID-TIMS technique. *Economic Geology*, 103, 465-471.
- Schmitz, M. D., and Schoene, B., 2007. Derivation of isotope ratios, errors, and error correlations for U-Pb geochronology using <sup>205</sup>Pb-<sup>235</sup>U-(<sup>233</sup>U)-spiked isotope dilution thermal ionization mass spectrometric data. *Geochemistry, Geophysics, Geosystems*, 8, Q08006, doi:10.1029/2006GC001492.
- Sigloch, K., Mihalynuk, M.G., 2013. Intra-oceanic subduction shaped the assembly of Cordilleran North America. *Nature* 496, 50-56.
- Sláma, J., Košler, J., Condon, D.J., Crowley, J.L., Gerdes, A., Hanchar, J.M., Horstwood, M.S.A., Morris, G.A., Nasdala, L., Norberg, N., Schaltegger, U., Xchoene, B., Tubrett, M.N., and Whitehouse, M.J., 2007. Plešovice zircon — A new natural reference material for U-Pb and Hf isotopic microanalysis. *Chemical Geology*, 249, 1-35.
- Stacey, J.S., and Kramers, J.D., 1975. Approximation of terrestrial lead isotopic evolution by a two-stage model. *Earth and Planetary Science Letters*, 26, 207-221.
- Stevenson, J.P., 2013. SeGO Resources Reports Drill Results and Presents a 3D Video Overview of Results to Date. October 11 News Release, 3 p. <http://www.segoresources.com/>.
- Sun, S.S., McDonough, W.F., 1989. Chemical and isotopic systematics of oceanic basalts; implications for mantle composition and processes. *Magmat. Ocean Basins* 42, 313-345.
- Tempelmann-Kluit, D.J., 1979. Transported cataclasite ophiolite and granodiorite in Yukon: evidence of arc-continent collision. Geological Survey of Canada, Paper 79-14, 27 p.
- Tafti, R., Mortensen, J.K., Lang, J.R., Rebagliati, M., and Oliver, J.L., 2009. Jurassic U-Pb and Re-Os ages for newly discovered Xietongmen Cu-Au porphyry district, Tibet: Implications for metallogenic epochs in the southern Gangdese Belt. *Economic Geology*, 104, 127-136.
- Thirlwall, M. F., 2000. Inter-laboratory and other errors in Pb isotope analyses investigated using a <sup>207</sup>Pb-<sup>204</sup>Pb double spike. *Chemical Geology*, 163, 299-322.
- Stevenson, J.P., 2013. SeGO Resources Reports Drill Results and Presents a 3D Video Overview of Results to Date. October 11 News Release, 3 p. <http://www.segoresources.com/>.
- Thorkelson, D.J., and Rouse, G.E., 1989. Revised stratigraphic nomenclature and age determinations for mid-Cretaceous volcanic rocks in southwestern British Columbia. *Canadian Journal of Earth Sciences*, 26, 2016-2031.
- Tribe, S., 2005. Eocene paleo-physiography and drainage directions, southern Interior Plateau, British Columbia. *Canadian Journal of Earth Sciences*, 42, 215-230. doi: 10.1139/e04-062.
- Whalen, J.B., Currie, K.L., Chappell, B.W., 1987. A-type granites: geochemical characteristics, discrimination and petrogenesis. *Contrib. Mineral. Petrol.* 95, 407-419.